



Guest editors:  
K. Buchanan and S. Staddon

Volume 46, Number 8, December 2018  
ISSN 0961-3218 (Print) 1466-4321 (Online)  
© 2018 Taylor & Francis



## Scale-adaptive morphometric analysis for urban air quality and ventilation applications

Laura S. Leo, Riccardo Buccolieri & Silvana Di Sabatino

To cite this article: Laura S. Leo, Riccardo Buccolieri & Silvana Di Sabatino (2018) Scale-adaptive morphometric analysis for urban air quality and ventilation applications, Building Research & Information, 46:8, 931-951, DOI: [10.1080/09613218.2018.1501797](https://doi.org/10.1080/09613218.2018.1501797)

To link to this article: <https://doi.org/10.1080/09613218.2018.1501797>



© 2018 The Author(s). Published by Informa UK Limited, trading as Taylor & Francis Group



[View supplementary material](#)



Published online: 14 Aug 2018.



[Submit your article to this journal](#)



Article views: 222



[View Crossmark data](#)

## Scale-adaptive morphometric analysis for urban air quality and ventilation applications

Laura S. Leo <sup>a</sup>, Riccardo Buccolieri <sup>b</sup> and Silvana Di Sabatino <sup>c</sup>

<sup>a</sup>Department of Civil & Environmental Engineering and Earth Sciences, University of Notre Dame, Notre Dame, IN, US; <sup>b</sup>Dipartimento di Scienze e Tecnologie Biologiche ed Ambientali, University of Salento, Lecce, Italy; <sup>c</sup>Department of Physics and Astronomy, University of Bologna, Bologna, Italy

### ABSTRACT

A novel, flexible method to derive urban morphometric parameters is presented. Through selected examples, it demonstrates its employability in a wide range of applications. This method builds upon an extension of an image-based technique for the treatment of building data to discuss objective criteria for model grid choice and related consequences. Starting from an estimation of aerodynamic parameters, and their validation by computational fluid dynamics using an existing simulation of downtown Oklahoma City in the US, the method is used to evaluate improvements in the performance of an operational dispersion model. Results are applied to flow over a neighbourhood for the determination of ventilation parameters. It is suggested that the grid used for calculation of morphometric parameters provides the best agreement with data from laboratory experiments when the selection of grid size is made upon the spatial profile of building height standard deviation and maximum building height. The implication is that when a mesoscale numerical model is employed, morphometric parameters should be calculated by positioning the computational grid based on physical boundaries, while for finer resolution (namely, smaller scale) numerical models, morphometric parameters should be calculated using the street grid as external boundary, and the maximum building height criterion performs well.

### KEYWORDS

air quality; built form; microclimates; urban design; urban form; urban planning; ventilation

### Introduction


Urban forms, the material of the built environment, shapes and the orientation of individual buildings are important features of the urban environment that contribute to modify the surface energy balance as well as flow and dispersion characteristics (Grimmond & Oke, 1999; Millward-Hopkins, Tomlin, Ma, Ingham, & Pourkashanian, 2013; Roth, 2000). Cities with their clusters of neighbourhoods, street networks and buildings' layouts determine the ventilation and pollution dilution potential at both city and intra-city scales (Carruthers, Di Sabatino, & Hunt, 2012; Di Sabatino, Buccolieri, & Kumar, 2018; Wang, Sandberg, Lin, Yin, & Hang, 2017). Recent literature (e.g. Kravtsov, Santiago, Martilli, Christen, & Oke, 2015; Aliabadi et al., 2017) has clearly confirmed the close linkages between the built form at the neighbourhood scale, building packing density and the microclimate. An urban planner may be interested in how to plan a new


neighbourhood with reduced energy consumption, or to maintain a good air quality level, or to keep the local air temperature under control. Common in the applications above is the use of morphometric parameters such as: the average building height,  $\bar{H}$  (weighted with the planar area); maximum building height,  $H_{\max}$ ; building height standard deviation,  $\sigma_H$ ; the planar area density,  $\lambda_p$ ; and the frontal area density,  $\lambda_f$ , for a given incoming wind direction  $\theta$ , with lambda parameters defined as:

$$\lambda_p = \frac{\sum_i A_{p,i}}{A_T}$$

$$\lambda_f = \frac{\sum_i A_{f,i}(\theta)}{A_T},$$

where  $A_T$  is the total site planar area;  $H_i$  and  $A_{p,i}$  are the height and planar area of the  $i$ th building respectively;

**CONTACT** Laura S. Leo  lleo1@nd.edu

 Supplemental data for this article can be accessed <http://dx.doi.org/10.1080/09613218.2018.1501797>.

© 2018 The Author(s). Published by Informa UK Limited, trading as Taylor & Francis Group

This is an Open Access article distributed under the terms of the Creative Commons Attribution License (<http://creativecommons.org/licenses/by/4.0/>), which permits unrestricted use, distribution, and reproduction in any medium, provided the original work is properly cited.

and  $A_{f,i}(\theta)$  is its frontal area projected into the plane normal to the incoming wind direction  $\theta$ .

Once these five parameters are known, the urban form associated with a specific neighbourhood is well characterized with respect to the incoming flow (Ratti, Di Sabatino, & Britter, 2006). From these parameters, aerodynamic parameters such as the aerodynamic roughness length,  $z_0$ , and the zero-plane displacement,  $z_d$ , which connect the surface characteristics with the flow and temperature profiles in the lower part of the atmospheric layer (Britter & Hanna, 2003) can be derived. Despite the determination of both  $z_0$  and  $z_d$  being rather established from the theoretical point of view (Fernando, 2000; Jackson, 1981; Kaimal & Finnigan, 1994; Tennekes, 1973), this is not an easy task in real applications (e.g. Wiernga, 1993). As recently reviewed by Kent et al. (2017), methods to estimate surface roughness characteristics include several based on morphometric analyses that provide good predictions of measured wind data with the provision that building height variability is included. This was first pointed out by Ratti et al. (2006) and later formally incorporated into novel aerodynamic roughness length formulations (e.g. Kanda, Inagaki, Miyamoto, Gryschka, & Raasch, 2013). Several areas of research use morphometric parameters. Crucial in atmospheric numerical modelling is the quantification of the horizontal transport through the canopy, vertical transport in-out canopy and boundary layer height, the last being the depth through which pollutants are diluted, and water vapour and heat which vary in response to the underlying surface properties. Air quality and thermal comfort at a given neighbourhood will be the result of how the dynamic components above contribute to the mean and turbulent transport of a given scalar (i.e. temperature, pollutant concentration, water vapour etc.). While studies on each of these dynamic components abound (for example, see the recent reviews by Barlow, 2014; Blocken, Tominaga, & Stathopoulos, 2013; and Ming, Peng, Gong, & Li, 2017), and so are the different approaches and methods adopted, more comprehensive analyses are rare and yet crucial to provide realistic urban scenarios as well as to deliver unique and broadly applicable tools, methods and criteria for specific applications. This study aims to be a step in such a direction while providing practical guidelines for use of the right grid spacing in non-building-resolving numerical models for air quality and microclimate when morphometric parameters are used. Specifically, its objectives are:

- to present a novel and scale-adaptive methodology based on image-processing techniques to calculate morphometric parameters in a spatially varying fashion
- to propose an argument for the choice of the calculation grid according to the numerical model used

- to show how the method works in practice by proving its robustness in selected examples.

Computational fluid dynamics (CFD) is used as a provider of benchmark data for the establishment of the fluid dynamics relevance of the morphometric parameters. Subtle in the calculation is the fact that when dealing with flow over an urban area, 'physical' neighbourhoods are blurred as the flow continuously evolves to adjust to the underlined surface (Barlow, 2014). Still, the notion of neighbourhood requires an a priori calculation of lambda parameters, mean building heights etc., which in turns requires an a priori and subjective choice of the area over which to normalize the building characteristics (frontal and planar area, building height etc.). To overcome this intrinsic problem, Mouzourides et al. (2014) introduced a method based on wavelet analyses. The signal associated with urban-building information was analyzed at different levels, each corresponding to a different scale. At each scale, the urban signal was decomposed into an approximation and a detail that was the part removed from the previous lower scale. The method allows a multi-scale representation of the urban information and shows a great potential for implementation in mesoscale models such as the Weather Research and Forecasting model (Ching et al., 2014). However, the method may be less effective when wind direction is taken into consideration; therefore, it cannot compute  $\lambda_f$  and its dependence with height which is crucial to capture the effect of building height in real cases typically exposed to large wind direction changes during the day. The method described herein includes wind direction changes while maintaining its scale-adaptive characteristics. It has several applications considering that morphometric parameters can be used in the determination of the drag force across the city (Buccolieri, Wigö, Sandberg, & Di Sabatino, 2017), which is useful for the assessment of natural ventilation (Nishizawa, Sawachi, & Maruta, 2008). Similarly, it can be used to determine *city breathability*, or simply *breathability*, that reflects the potential of a city to dilute pollutants and is directly related to the air flow pattern determined by the interaction between the approaching wind and the city itself (Buccolieri, Sandberg, & Di Sabatino, 2010; Panagiotou, Neophytou, Hamlyn, & Britter, 2013). In many breathability studies (e.g. Buccolieri, Salizzoni, Soulhac, Garbero, and Di Sabatino, 2015; Panagiotou et al., 2013; Salizzoni, Soulhac, & Mejean, 2009) the notion of the exchange velocity (i.e. a bulk quantity that includes all the contributions to the vertical transfer of mass through the canyon roof) is used in combination with the in-canopy velocity scale, a bulk scale that can be easily derived from morphometric parameters (Bentham

& Britter, 2003; Solazzo, Di Sabatino, Aquilina, Dudek, & Britter, 2010; Soulhac, Salizzoni, Mejean, & Perkins, 2013; Kubilay, Neophytou, Matsentides, Loizou, & Carmeliet, 2017). Although simplified methods for both exchange and in-canopy velocity have been based on simple arrays of buildings, the novel morphometric method proposed here makes them applicable to highly inhomogeneous urban geometries.

Following the objectives and the rationale, the paper is structured as follows. After the introduction, the methodology for the treatment of urban form is explained and a series of applications (ventilation and pollutant dispersion) are presented and discussed. The applications shown use morphometric parameters whose correct calculation is relevant to urban design as well in flow and dispersion models at the neighbourhood, city scale and mesoscale.

### Method for the analysis of heterogeneous building arrays

The morphometric method presented herein is an extension of the methodology of Di Sabatino, Leo, Cataldo, Ratti, and Britter (2010). It follows that an urban digital elevation model (DEM) can be represented as a raster image in grey scale of dimension (in pixels)  $p_x$  and  $p_y$ , where the number assigned to each pixel (*i.e.* its grey tonality) represents the height above the ground. It is a two-dimensional matrix of height values where the position of each matrix element (*i.e.* each pixel) is implicitly associated with planar spatial coordinates (Figure 1). The relation between horizontal dimensions  $s_x$  and  $s_y$  (in meters) of the urban area and the image dimension is given by the scale factor:  $\beta = s_x/p_x = s_y/p_y$  m/pixel. As

such, it can be considered just a digital image and analyzed with digital image-processing techniques to calculate morphometric parameters such as  $\lambda_p$ ,  $\lambda_f(\theta)$ ,  $\bar{H}$ ,  $H_{\max}$  and  $\sigma_H$ . The method implicitly requires an ad-hoc preselection of the urban portion over which the morphometric analysis has to be performed. The following procedure overcomes this limitation by allowing the computation of  $\lambda_p$ ,  $\bar{H}$ ,  $H_{\max}$ ,  $\lambda_f$  and  $\sigma_H$  as a function of the spatial coordinates  $(x, y)$  of the domain. Indeed, analogous to the idea of calculating lambda parameters as a function of elevation  $z$  discussed by Di Sabatino et al. (2010), these morphometric parameters can be calculated as a function of the horizontal variables  $x$  and  $y$ .

Let  $x$  and  $y$  denote the along-row and along-column direction of the image matrix respectively (Figure 1), and assume for simplicity a wind vector blowing along the positive  $x$ -axis. The approach consists of dividing the image into a grid and then performing a morphometric analysis on each grid cell of dimension  $\Delta x$  and  $\Delta y$ . The grid construction is performed by using a simple algorithm that relies on the constants of proportionality  $\beta$  between the real planar dimension of the city and the matrix dimension. The procedure is described in detail in Appendix A in the supplementary online data. The grid itself can be either regular or irregular and made of either rectangular or squared grid cells. Incidentally, the similitude with the grid construction in numerical weather and air-quality models is striking, thus enabling the user to compute the morphometric parameters at the spatial resolution that best matches that of the computational model. This is one advantage of the method proposed here. On the other hand, this tool may help guide model horizontal resolution choices, its great strength being the ability of investigating morphological intra-

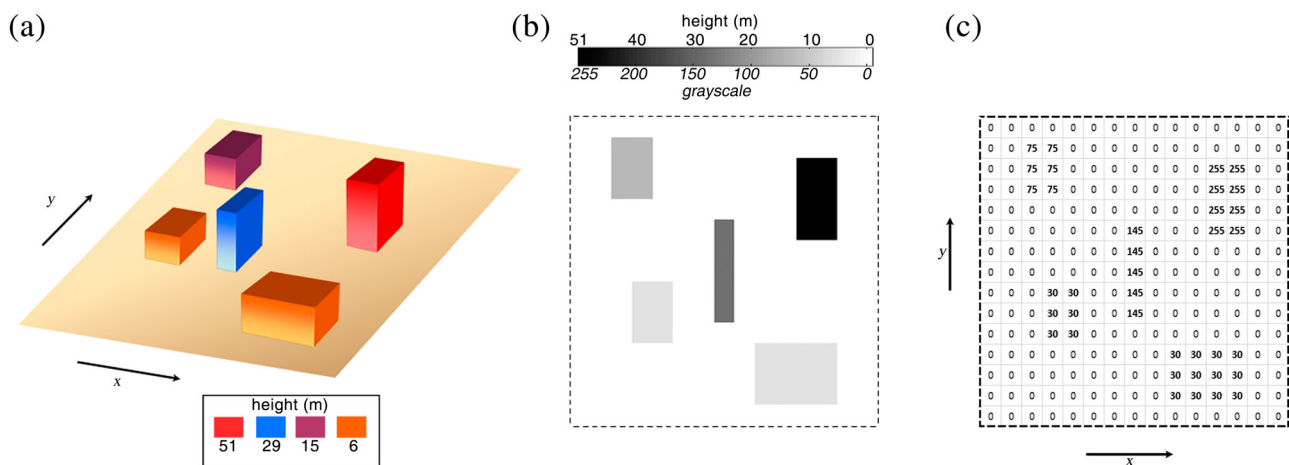


**Figure 1.** Schematic showing the equivalence between (a) a three-dimensional urban digital elevation model (DEM), (b) its representation as a greyscale raster image and (c) its representation as a two-dimensional matrix. The colourmap in (b) shows the correspondence between the 256 shades of grey (from 0 to 255) and the building heights (from 0 to 51 m) adopted in this example, namely, a ratio  $\alpha = [\text{height/shade of grey}] = 0.2$  m.

city variations and identifying ‘physical’ neighbourhoods, namely the portion of the city with horizontally homogeneous morphometric characteristics (Di Sabatino, Solazzo, Paradisi, & Britter, 2008). If this is the objective, then the choice of the image grid spacing  $\Delta x$  and  $\Delta y$  is no longer arbitrary, but dictated by the characteristic length scale of the ‘physical’ neighbourhood itself. To identify this length scale, hence, the appropriate grid spacing, the image-based analysis has to be first performed using a step  $\Delta x = \Delta y$ , such that  $\Delta x \ll s_x$  and  $\Delta x \sim \beta$ . This allows one to capture the spatial variation of the urban area in a continuum fashion rather than as bulk information intrinsically affected by the choice of  $\Delta x$  or  $s_x$ . For the same reason, the results obtained from this fine-scale analysis should be interpreted only in terms of ‘raw’ morphometric information, namely height information (the value of each pixel) and/or planar built area information (the count of non-zero pixels) (‘raw’ as opposed to information derived through further calculation or manipulation of the image which requires normalization over the domain). Here the focus is on height-based information. Specifically, the fine-scale analysis is used to investigate the spatial variation of  $\sigma_H/\bar{H}$  and  $H_m/H_{\max}$ , the latter being the ratio between local maximum building height,  $H_m$ , and the maximum height,  $H_{\max}$ , associated with the entire domain. (Note that  $H_m/H_{\max} = 0$  automatically identifies a major air corridor, such as a street.) The optimal image-grid spacing  $\Delta x$  and  $\Delta y$  is then identified by the contiguous regions of the domain with relatively similar values of these ratios. Additional constraints may be imposed depending on the specific application. In a mesoscale model, for example, the requirement will be neglecting intra-city variations  $\Delta x$ ,  $\Delta y$  that are smaller than the numerical grid resolution. This choice of  $\sigma_H/\bar{H}$  and  $H_m/H_{\max}$  is motivated by the need to account for the vertical building height variability, which largely modifies the overall drag exerted on the flow by the buildings (e.g. Kanda et al., 2013, *passim*), with the tallest buildings having a dominant effect (Xie, Coceal, & Castro, 2008). Alternative criteria are of course possible. For example, an area could be partitioned in correspondence of streets or air corridors. This choice may be preferable when looking at applications at the neighbourhood scale or smaller (the partition of a single neighbourhood into subregions), given that a street canyon represents the characteristic urban-length scale at the intra-neighbourhood scale.

In summary, the criteria discussed above are based on theoretical considerations and tested here on a single case study. The provision of general guidelines would require a robust validation on a large data set of urban domains of different size and morphology, which is a work in progress by the authors.

## Application of the method to the test case

The area used as a test case is downtown Oklahoma City (OKC) in the US for which detailed geometry and experimental data were available from the European project COST Action 732 (Di Sabatino et al., 2011). The purpose of this study is threefold:

- to further illustrate the morphometric approach proposed in this paper
- to assess the fluid dynamics relevance of the calculated aerodynamic parameters derived from morphometric ones by comparison with results from detailed CFD simulations
- to evaluate potential improvements to the performances of operational numerical models routinely used for predicting flow and dispersion in urban environments: specifically, dispersion calculations for the Oklahoma case are performed using the non-CFD dispersion model ADMS-Urban (Atmospheric Dispersion Modelling System) (CERC, 2017) and the results are compared with wind tunnel (WT) data available from studies carried out in the Environmental Wind Tunnel Laboratory at Hamburg University, Germany (Leitl, Pascheke, Schatzmann, & Kastner-Klein, 2003).

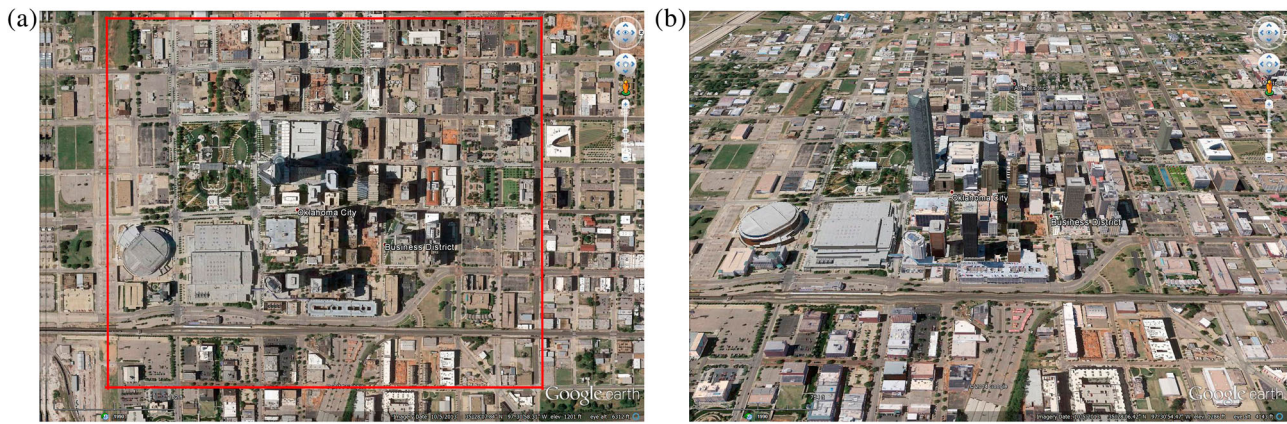
## Morphometric analysis

Figure 2(a) shows an aerial view of downtown OKC for which a three-dimensional (3D) view is given in Figure 2 (b). The area size is  $(s_x \times s_y) = (1260 \text{ m} \times 1050 \text{ m})$  and is characterized by a few high-rise buildings surrounded by a large number of shorter buildings, as typical in the business district of US cities. The maximum building height is 152 m.

The morphometric analysis of OKC starts by converting the initial 3D computer-aided design (CAD) map available from COST Action 732 into a raster image in grey scale (Figure 3). The resulting eight-bit image has dimensions  $(p_x \times p_y) = (3126 \times 2605 \text{ pixels})$ , corresponding to a scale factor of  $\beta = s_x/p_x = s_y/p_y \approx 0.5 \text{ m/pixel}$ . The scale between the 256 levels of grey scale and the building heights (m) was 1:1 (i.e.  $\alpha = 1$ ), so that, for example, a height of 152 m corresponds to a value of 152 in the image matrix. Here and in the following analysis, a wind vector blowing along the positive  $x$ -axis was selected in order to match the configuration of the experiments in the WT as well as of the numerical simulations.

First, a standard morphometric analysis over the entire DEM was performed (hereafter, Test1). As shown in Table 1, the relatively small values of  $\lambda_f$  ( $\theta$ ) and  $\lambda_p$  fall in the wake interference flow regime (Oke, 1987). The average building height is also low (26 m),





**Figure 2.** (a) Ariel image of downtown Oklahoma City (35°28′06.42″ N, 97°30′54.47″ W) with an indication of the study area (box); and (b) a three-dimensional representation of the same area.

Source: Author's screenshot of Google Earth.

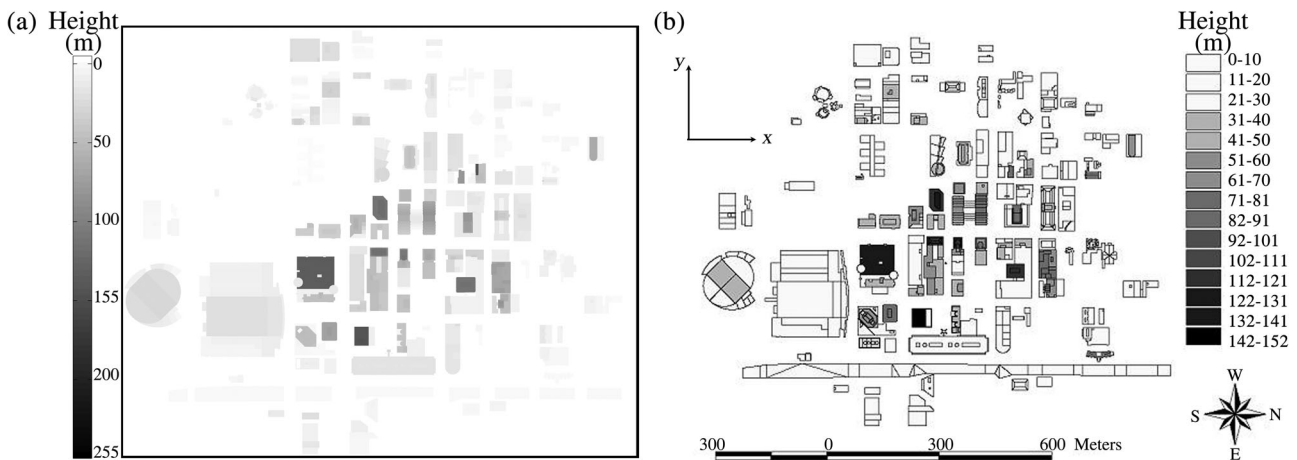


**Figure 3.** (a) Raster image of Oklahoma City used for the morphometric analysis. The scale between the 256 levels of grey scale and the building heights (m) is  $\alpha = 1$ ; and (b) for clarity, the same area is represented with a different greyscale.

but with a large standard deviation ( $\sigma_H/\bar{H} = 1.1$ ) as a reflection of having a considerable number of buildings distributed within a large range of heights. In this regard, we will show that the method presented here and applied in the following tests allows accounting for both building height distribution and the spatial variation of the other morphometric parameters.

A fine-scale image-based analysis was first performed ( $s_x \approx 1$  km and  $\beta = 0.5$  m/pixel, therefore a step of 1 m was chosen) to capture the vertical urban shape. Results from this fine-resolution analysis are illustrated in Figure 4, which shows the variability in terms of  $\sigma_H/\bar{H}$  and  $H_m/H_{max}$ . Three regions are easily detectable both along  $x$

and  $y$  directions suggesting an ad-hoc choice of the image partition (the solid red lines in Figure 4): two external regions  $H_m/H_{max} < 0.5$  and  $\sigma_H/\bar{H} < 1$ , and an intermediate region with  $H_m/H_{max} \gtrsim 0.5$  and  $\sigma_H/\bar{H}$  generally closer to 1.

Based on the grid identified above, two different tests were carried out over the OKC domain, namely Test2 and Test3. Test2 (not shown here) was performed to estimate one-dimensional (1D) spatial variation along the wind direction of the morphometric parameters, e.g.  $\lambda_f = \lambda_f(x)$ , while Test3 consisted of computing the same morphometric parameters as a two-dimensional (2D) discrete function of  $(x, y)$ . The grid spacing chosen in Test3 is mainly guided by  $H_m/H_{max}$ . A further refinement of the above grid is, however, possible, by isolating the portion with  $\sigma_H/\bar{H} < 1$  in the intermediate region along the  $x$  direction (the dashed red lines in Figure 4). 2D spatial morphometric variations were also computed for this refined grid (Test3b respectively). As mentioned,

**Table 1.** Building statistics for downtown Oklahoma City with respect to a wind blowing along the positive  $x$ -axis.

$\bar{H}$ (m)	$\lambda_p$	$\lambda_f(\theta)$	$z_d$ (m)	$z_0$ (m)
26	0.23	0.12	12.00	1.36

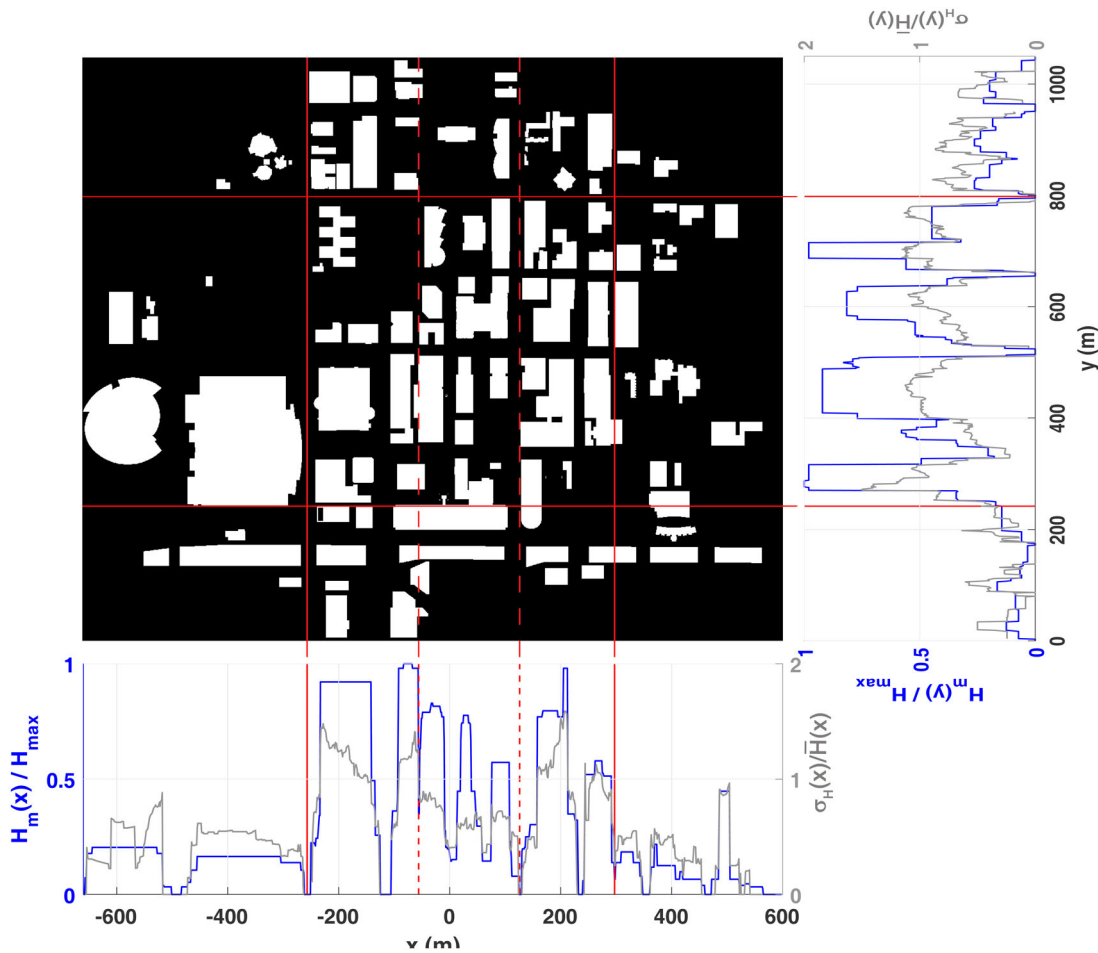


**Figure 4.** Fine-scale image-based analysis showing the variability in terms of  $\sigma_H/\bar{H}$  and  $H_m/H_{max}$ .

another possible criterion for the choice of the grid spacing is to select DEM ‘slices’ in correspondence of streets or air corridors, especially for relatively small domains such as OKC. This specific criterion was applied in the present study; relatively to  $\Delta x$  in Test2S and to both  $\Delta x$  and  $\Delta y$  in Test3S.

In Test2S,  $\Delta y$  was obviously chosen as a constant and equal to  $s_y$ , *i.e.* the whole DEM extension along the transversal direction  $y$ , since we were only interested in morphometric variations along the wind direction ( $x$ ). The

exact procedure to extrapolate the morphometric parameters for Test2S and Test3S are reported Tables A1 and A2 in Appendix A in the supplemental data online; the two resulting DEM partitions are shown in Figure 5.

Here, only the results of the street-based morphometric analysis are discussed in details as an illustrative example, while differences with the other approach will be discussed in the results section below.

Figure 6(a) shows the spatial distribution of various morphometric parameters such as  $\bar{H}$ ,  $\lambda_p$  *etc.* based on

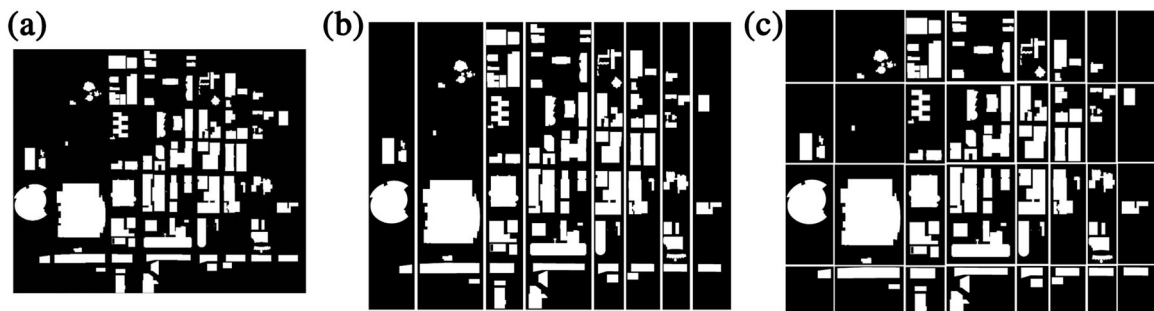


**Figure 5.** Grid adopted for the Oklahoma City geometry in (b) Test2S and (c) Test3S. For reference, the city’s geometry is shown in (a).

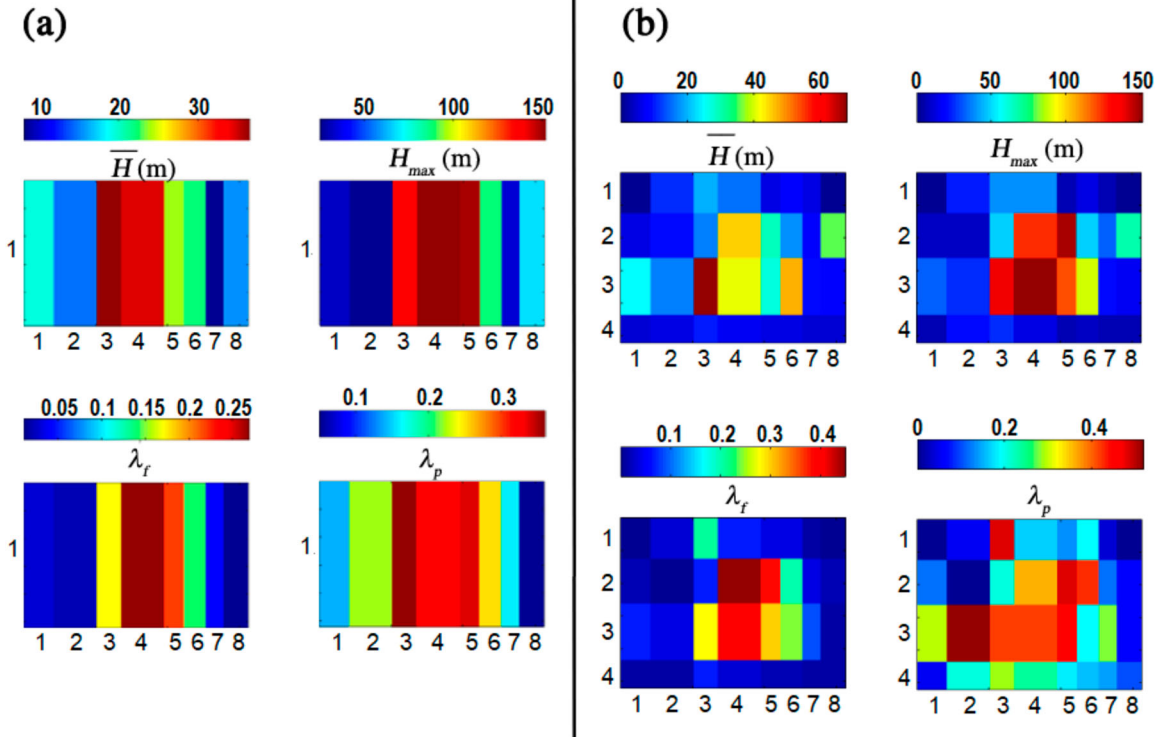


**Figure 6.** Spatial distribution of average building height  $\bar{H}$ , maximum building height  $H_{max}$ , planar area density  $\lambda_p$ , frontal area density  $\lambda_f$ , obtained from (a) Test2S and (b) Test3S. The  $x$  and  $y$  labels of each map denote the indices  $i, j$  of the submatrices  $M_{ij}$  over which the morphometric analysis was performed.

the image analysis carried out on each submatrix of Test2S (for details, see also Table A3 in Appendix A in the supplemental data online).

The finer grid associated with Test3S adds further details to the urban texture of OKC in terms of morphometric characteristics (Figure 6(b); see also Table A4 in Appendix A in the supplemental data online). In particular, the map of  $\lambda_p$  reveals a more scattered pattern with a peak of about 0.5 in some regions. On the other hand, low values of building height and frontal density characterize the outer portion of the domain, thus leading to smaller values of roughness length and zero-plane displacement.

#### Application: derivation of aerodynamic parameters

As previously stated, morphometric parameters can be used for the estimation of aerodynamic parameters ( $z_0$ ,  $z_d$ ) which are routinely used in dispersion models or urban flow models. Also, there are urban parameterizations within mesoscale models (e.g. Martilli, Santiago, & Salamanca, 2015) that use morphometric parameters directly in place of roughness length-based parameterizations. In both cases, the computation of morphometric parameters as a function of the horizontal urban

dimensions is an advantage. Indeed, the potential improvement in using a spatially varying aerodynamic roughness length in operational dispersion models such as ADMS has been rather established (Barnes et al., 2014). The image-based method presented here allows computing spatially varying  $z_0$  (and zero-plane displacement  $z_d$ ) based on any morphometric-based formulations available in the literature, such as those proposed by Macdonald, Griffiths, and Hall (1998) (hereafter [MA]), Kastner-Klein and Rotach (2004) (hereafter [KR]), and Kanda et al. (2013) (hereafter [KA1] and [KA2]), given as follows:

$$[\text{MA}]: \frac{z_0}{\bar{H}} = \left[ 1 - \frac{z}{\bar{H}} \right] \exp \left\{ - \left[ \frac{0.5 \beta_0 C_D \lambda_f}{\kappa^2} \left( 1 - \frac{z_d}{\bar{H}} \right) \right]^{-0.5} \right\}$$

with  $\alpha = 4.43$ ,  $\beta_0 = 1.0$ ,  $\kappa = 0.4$ ,  $C_D \sim 1$  and  $z_d/\bar{H} = 1 + (\lambda_p - 1)\alpha^{-\lambda_p}$ .

$$[\text{KR}]: \frac{z_0}{\bar{H}} = 0.072 \lambda_p \left[ \exp \{ -2.2 (\lambda_p - 1) \} - 1 \right]$$

$$[\text{KA}]: z_0 = z_{0[\text{ma}]} (bY^2 + cY + a)$$

with  $Y = \sigma_H \lambda_p / \bar{H}$  and  $(a, b, c) = (0.71, 20.21, -0.77)$  for [KA1] and  $(a, b, c) = (0.93, 8.93, 4.68)$  for [KA2].

Note that, unless otherwise specified, [MA] formulae were used in the analysis.



Results of the morphometric analysis conducted for Test1 (Table 1) show that OKC is characterized by a roughness length of 1.4 m and a displacement  $z_d$  of 12 m according to [MA]. From the morphometric results of Test2S variations of  $z_0$  along the wind direction, *i.e.*  $z_0 = z_0(x)$  were obtained, while Test3, Test3b and Test3S allowed computing  $z_0$  as a 2D discrete function of  $(x, y)$ .

As expected from [MA] formulation (Figure 7), the  $x$ -variation of  $z_d$  reflects quite well those of  $\bar{H}$  and  $\lambda_p$ , while the spatial distribution of  $z_0$  show similar patterns to  $\lambda_f$ . In particular, the spatial variation in aerodynamic roughness length along the  $x$  direction appears rather symmetric with respect to the centre of the domain, and goes from a first region of low roughness ( $z_0 < 1$  m) at the beginning and end of the domain followed by intermediate regions of larger roughness ( $z_0 \sim 1.5$  m) till a maximum of  $z_0 \sim 3$  m in correspondence of the central portion of the domain. The  $x$ -variation of  $z_d$  is slightly different, being characterized by a sharp increase from  $z_d \sim 6$  m at the beginning of the domain to  $z_d \sim 20$ – $23$  m in the remaining left half of the area. On the right half, the variation of  $z_d$  is more gradual, going from about 20 m to about 15 m, then about 11 m and down below 2 m. The finer grid associated with Test3S adds further details to the spatial variations in surface roughness, which are expected to affect the ability of operational numerical models to predict flow and dispersion over OKC area. This will be discussed in the results section.

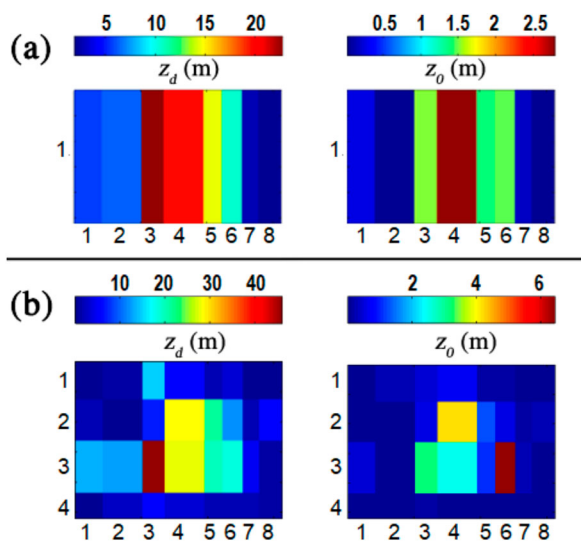


**Figure 7.** Spatial distribution of zero-plane displacement height  $z_d$ , and roughness length  $z_0$ , derived from Macdonald, Griffiths, and Hall's (1998) equations using the morphometric parameters obtained for (a) Test2S and (b) Test3S.

### CFD simulations for method assessment

3D isothermal steady-state flow and pollutant dispersion simulations were performed by means of the CFD code FLUENT within the project COST Action 732 (2005–09; see [http://www.cost.eu/COST\\_Actions/essem/Actions/732](http://www.cost.eu/COST_Actions/essem/Actions/732)), which reproduced the WT experiment carried out in the Environmental Wind Tunnel Laboratory (model scale 1:300). Full results are reported in Schatzmann, Olesen, and Franke (2010).

The simulated area develops around the business district of OKC. Figure 8(a) shows the computational domain and 768 individual buildings explicitly described. The wind blows along the positive  $x$ -direction. In full scale, the highest building has a height of  $H_{\max} = 152$  m, thus 912 m (*i.e.*  $6H_{\max}$ ) was chosen as the height of the computational domain. The distance between the last building and the outlet was approximately  $6.6H_{\max}$  along the  $x$ -direction. From the highest building the distance was approximately  $11H_{\max}$ . The distance between the inlet and the first building was  $1.3H_{\max}$ , which corresponds to five times the height of the first buildings.

Simulations were made at model scale using an unstructured grid with about 14 million tetrahedral cells. The standard  $k$ - $\epsilon$  turbulence model (Launder & Spalding, 1974) was used with standard wall functions. The boundary conditions were symmetry at the domain sides and top and a constant pressure at the domain outlet. At the inlet, velocity component, turbulent kinetic energy (TKE) and turbulent dissipation rate ( $\epsilon$ ) were prescribed as derived from WT data, yielding a power law for the velocity component in the  $x$ -direction and a second-order polynomial for the TKE up to  $z = 386$  m and constant above:

$$U(z) = U_{\text{ref}} \left( \frac{z}{z_{\text{ref}}} \right)^{0.18} \quad (1)$$

with the undisturbed reference velocity  $U_{\text{ref}} = 8.84 \text{ m s}^{-1}$  at  $z_{\text{ref}} = 40.2$  m (full scale). The turbulent dissipation rate was set equal to the production of the TKE.

The ground source was located in Park Avenue at full-scale position  $(x, y, z) = (-6.22, -80.08, 4.00 \text{ m})$ , where the measurement positions were also located (see the results section), and was modelled as a volume source (Figure 8(b)). The minimum experimental volume flow rate equal to 0.3 l/h was set. The turbulent scalar flux in the transport equation for the passive scalar was modelled by the gradient diffusion assumption, with a turbulent Schmidt number  $Sc_t = 0.7$ . The numerical approximations for the advective terms used the second-order upwind interpolation for the pressure and the momentum, and the first-order upwind interpolation for the turbulence equations. The iterative

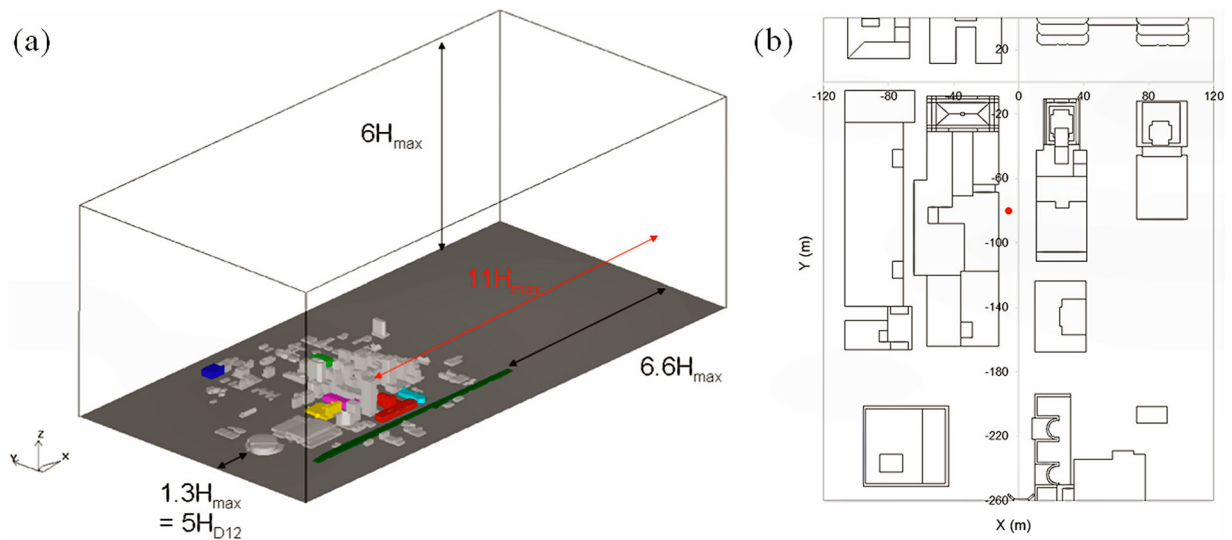


**Figure 8.** (a) Computational domain for Oklahoma City computational fluid dynamics (CFD) simulation.  $H_{D12}$  is the height of the oval building closest to the inlet;  $H_{max}$  the height of the tallest building; and (b) sketch of the geometry showing the position of the source (red point) in Park Avenue; dimensions are in full scale.

Source: Schatzmann et al. (2010).

convergence was attempted to reach below  $10^{-6}$  for the flow (Schatzmann et al., 2010). Although this value was not achieved exactly, because of the tetrahedral mesh and the usage of the single precision solver, simulations were run until the residuals became constant, which was estimated to be acceptable. Specifically, the residuals for the continuity equation and  $\epsilon$  were equal to about  $5 \times 10^{-5}$ , while residuals for the velocity components and TKE were just below  $1 \times 10^{-6}$ . These values were reasonable enough to trust the simulation results for further analyses. Simulations took about four to five days by using a workstation with 32GB RAM and 8 CPU.

### Application: air quality model

Dispersion calculations for OKC were also performed (in full scale) using ADMS-Urban (CERC, 2017). Note that in this model buildings (when not explicitly resolved) are accounted for by increasing the aerodynamic roughness length using a single spatially averaged value or a distribution of roughness lengths. The choice of the roughness length has a significant effect on the calculated concentrations. The ADMS-Urban can make use of the FLOWSTAR model to carry out dispersion calculations over a change of roughness using a linearized perturbation theory approach similarly to that used for flow over hills (Jackson & Hunt, 1975). This is equivalent to modelling the flow over a change of surface roughness, which can be either a step change or a smooth variation of surface roughness. The latter can be considered as a caveat within non-CFD models to take into account the effect of flow adjustment over the urban surface. In the present study

both methods (*i.e.* step change and smooth variation of surface roughness) were used. The difference between the runs was mainly the way the authors modelled the surface roughness change in the area occupied by the array of buildings, while in the area upwind of the array the same  $z_0$  as in the CFD modelling was used. The characteristics of the runs were (all dimensions are in full scale):

- Run\_1 was performed using the single fixed roughness of 1.36 m obtained in Test1 for the whole area of OKC. A simple roughness step change from  $z_0 = 0.24$  to 1.36 m was used.
- Run\_2 was performed using a spatially varying roughness  $z_0 = z_0(x, y)$  obtained in Test3, Test3b and Test3S respectively.
- Run\_3 was performed using a spatially varying roughness  $z_0 = z_0(x, y)$  computed according to the wavelet analysis proposed by Mouzourides, Kyprianou, and Neophytou (2013). The test presented here is denoted lev7 and represents Level 7 in Mouzourides et al. (2013, fig. 7). Note that the additional levels reported by authors were also evaluated (data not shown).
- Run\_4 was performed using an additional group of tests, TestsR1–R5, to evaluate the sensitivity of the model with respect to the DEM grid spacing as well as different roughness formulations.

The point source was positioned at the same position as in CFD simulations. As an example, carbon monoxide (CO) was considered with an emission rate  $Q = 1$  g/s. The meteorological data was the same considered in the WT, *i.e.* a wind speed of 8.84 m/s at  $z = 40.2$  m

(full scale). Concentrations were normalized as follows.

$$K = \frac{CU_{\text{ref}}h^2}{Q} \quad (2)$$

where  $C$  is the calculated concentration; and  $h = 300$  m. Concentrations were compared against the Hamburg WT measurements.

## Results

Results of the CFD simulations performed on downtown OKC (with no built-form reduction) are used here to investigate the effects to the flow induced by the real urban geometry and assess the fluid dynamics' relevance of the morphometric method proposed in this paper. This is relevant to show that the method aiming to reduce the number of buildings in a specific region is reasonable in terms of the validity of the new parameters associated with the modified procedure.

### Effects of buildings on mean flow and dispersion

To verify the robustness of the proposed method, WT data available from studies carried out in the

Environmental Wind Tunnel Laboratory are taken into account. Measurements were in particular performed close to Park Avenue where the ground source was located. The general location of the flow and concentration measurement planes and points are shown in Figure 9. Overall, 2824 flow measurement positions, each with two components of the mean velocities and three components of the Reynolds stress tensor, and 683 concentration measurement positions were considered.

As an example, velocity results are shown for the measurement plane  $z = 10$  m (Figure 10). Fluid enters Park Avenue from both sides. At the corners weak recirculation regions are visible, but part of the flow is already parallel to the building walls aligned with the  $y$ -axis. This parallel flow in a negative  $y$ -direction quickly extends over the entire street width. Above the ground source, shown with a red cross, the flow direction is towards negative  $y$ -values. The CFD simulations provided a different flow field at  $z = 10$  m, with a better agreement in the lower part of the street. With increasing height the differences between the measured and calculated horizontal flow fields get smaller. In particular, differences become smaller with increasing height and at  $z = 80$  m the agreement between both simulations and the measurements is good (Schatzmann et al., 2010).

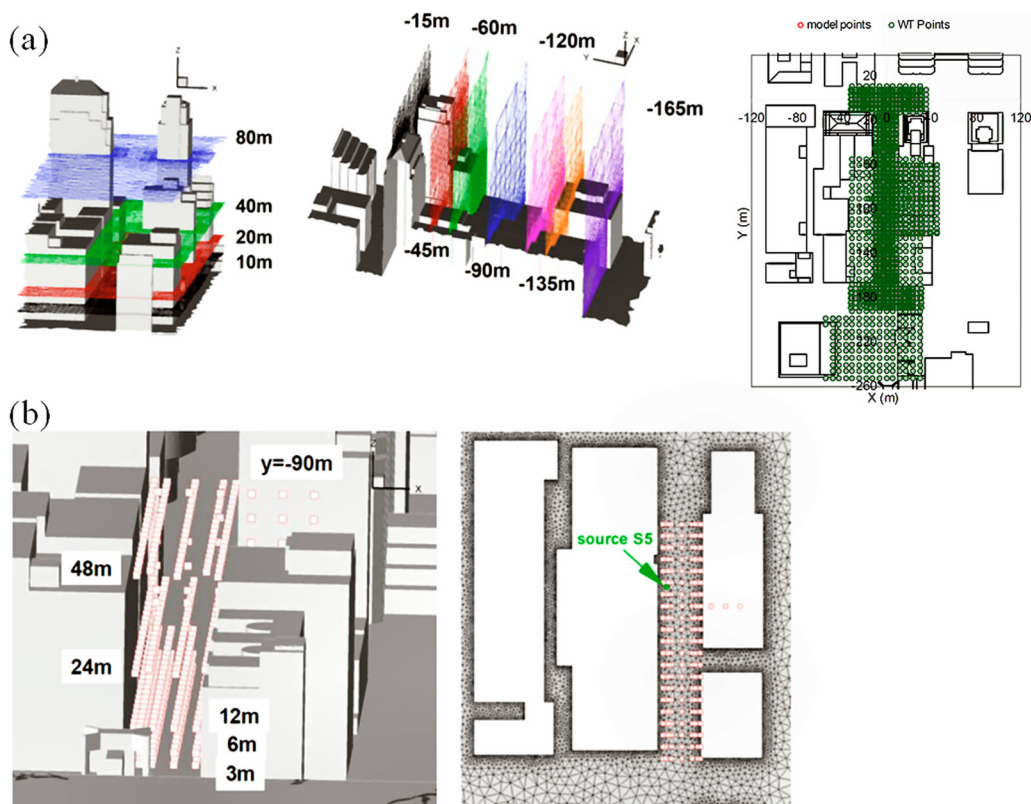


**Figure 9.** (a) Velocity measurement planes and positions; and (b) concentration measurement positions in Park Avenue. Dimensions are in full scale and the flow is along the positive  $x$ -direction.

Source: Schatzmann et al. (2010).

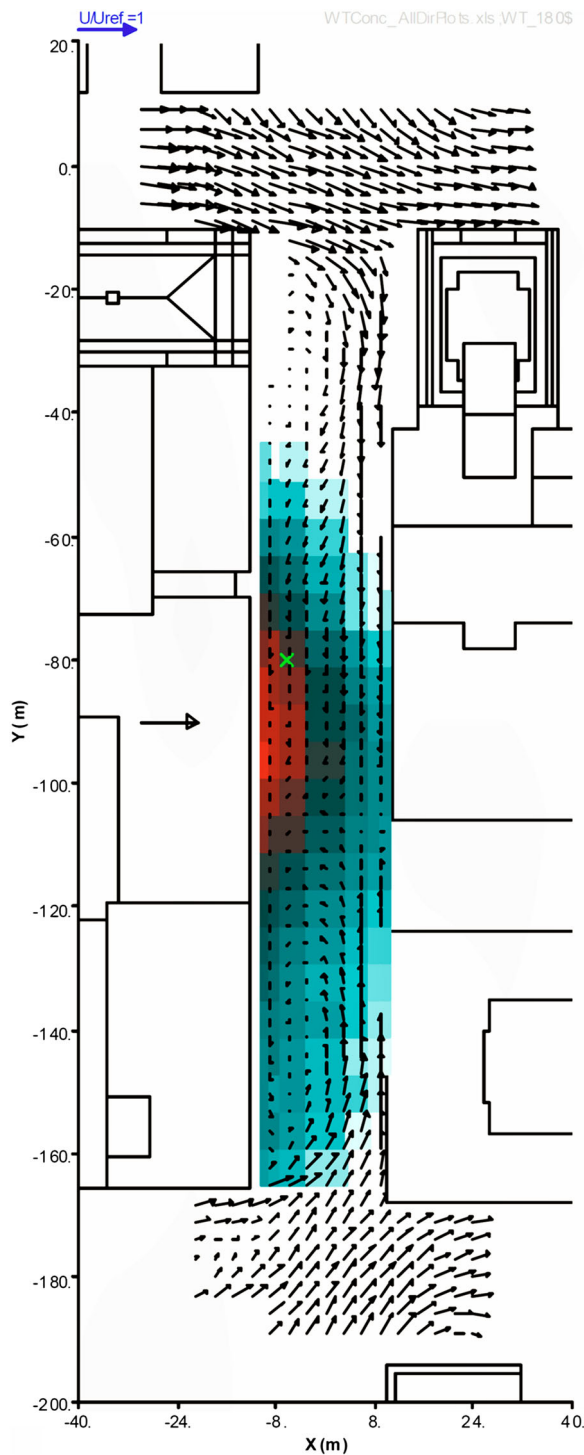


**Figure 10.** Measured velocity field at  $z = 10$  m and dimensionless concentration field at  $z = 3$  m. The green cross indicates the ground-source location. Dimensions are in full scale.

Source: Schatzmann et al. (2010).

It is known that large eddy simulations (LES) perform better in predicting turbulence than Reynolds-averaged Navier–Stokes (RANS) models (Liu, Ng, & Wong, 2015). However, steady RANS approaches have been shown to successfully predict the spatial distribution of mean velocity and concentration fields. They are in

fact still widely used to investigate the main features characterizing the mechanics of ventilation in street canyons and urban canopies, as recently done in the comprehensive evaluation exercises within the COST Action 732 (Di Sabatino et al., 2011). Among RANS, literature studies found that the differences in the results between the standard  $k-\epsilon$  (that employed here) and the modified  $k-\epsilon$  models are rather small for dispersion in street canyons and building complexes, where turbulence produced by surrounding buildings is dominant (Tomimaga & Stathopoulos, 2013), as happens in the present case. To gain further confidence in CFD simulations, several standard metrics were calculated, namely the mean, the fraction of predictions within a factor of two of observations (FAC2) and the correlation coefficient ( $R$ ) (Figure 10). According to COST Action 732 (Di Sabatino et al., 2011), the recommended criterion is  $FAC2 \geq 0.5$  (Figure 11). The CFD could not predict well the vertical component of the velocity ( $W$ ) since the standard  $k-\epsilon$  model over-predicted the TKE near the upwind corner of buildings which excessively mixed the flow and arrested the vertical velocity component. Figure 10 shows an overall better agreement for the horizontal velocity components ( $U$  and  $V$ ) (Schatzmann et al., 2010). The present authors considered it acceptable to employ such simulations as an example to apply the morphometric method to extract spatially varying roughness to be used as an input into the dispersion model. In fact, one needs to capture the mean features of the flow to be used for the subsequent analyses. In future, the authors intend to make further steps and improve the CFD predictions and extend the analysis to other urban building data sets covering different cities.

#### **Estimation of $z_0$ by CFD log profiles and the morphometric approach**

The CFD vertical profiles of the flow speed  $U$  (averaged along the span-wise  $y$ -direction between  $-600$  and  $600$  m corresponding to the transversal size of the building array) were extracted at several positions downstream (every 10 m) along the  $x$ -direction and compared with the upstream profile  $U_0$  (the blue line in Figure 12). As the airflow encounters the urban surface, it either slows down because of the increased surface friction (smooth–rough) or speeds up as the surface friction reduces (rough–smooth). The effect of this deceleration or acceleration is diffused vertically by turbulence and the effect of the change determines the growth of an internal boundary layer. Theoretically, the vertical wind profile in the upper portion of the layer is logarithmic and displays characteristics of the downwind surface



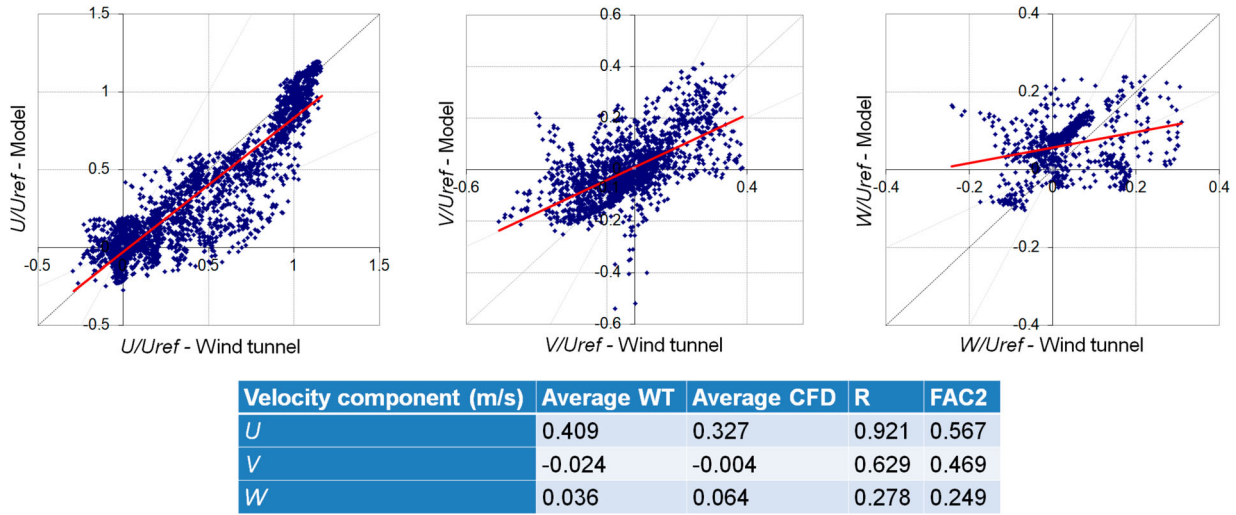


**Figure 11.** Scatter plots and metrics comparing velocity components obtained from computational fluid dynamics (CFD) simulations with wind tunnel (WT) data at the measurement positions.

through the new  $z_0$ , and the displacement height  $z_d$ :

$$U(z) = \frac{u_*}{\kappa} \left( \frac{z - z_d}{z_0} \right) \quad (3)$$

where  $u_*$  is the friction velocity. Figure 12 shows these profiles reported in a semi-log scale. For each profile, at a given height  $z$ , the velocity represents the average along the  $y$ -direction. Each subplot shows the profiles at two given positions  $x_1$  and  $x_2$ . An average of all profiles

extrapolated between  $x_1$  and  $x_2$  is also included (the red curve). Remember that in a semi-log plot the log-law becomes a straight line with a slope of  $u_*/\kappa$  and intercept  $(z_0 + z_d)$ , the presence of a log-law region departing from the upstream profile can be easily recognized for which an estimation of  $(z_0 + z_d)$  can be obtained.

Overall, three different behaviours of the flow can be recognized. As shown in Figure 12, there is an initial region where the flow is clearly evolving until it reaches

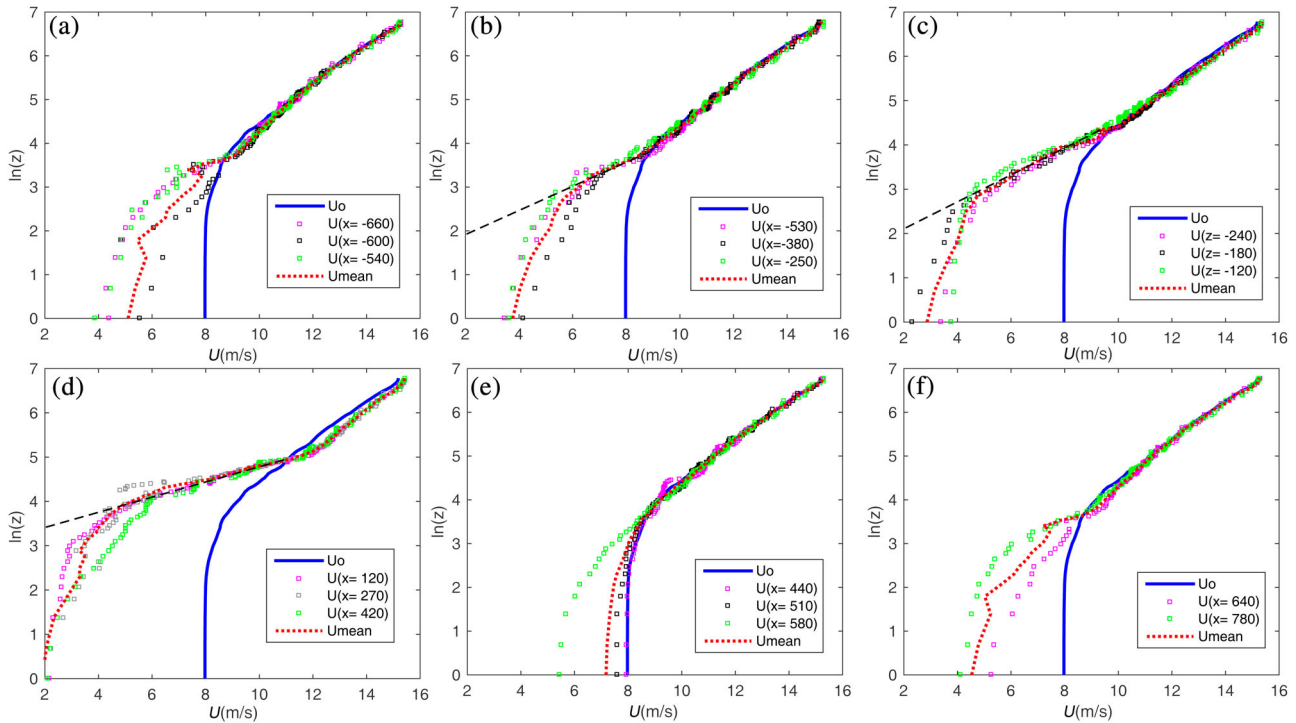


**Figure 12.** Semi-log plot of mean velocity profiles. The inlet profile at  $x = -840$  m is also given for reference. The black line denotes the slope of a plausible log-law profile, characteristic of the upper region of the internal boundary layer. The intercept with the  $y$ -axis represents  $\ln(z_0 + z_d)$ .

a first-equilibrium phase where a log-law region corresponding to  $\ln(z_0 + z_d) \approx 2$  is also visible. Due to the inhomogeneous nature of the underlying surface, the flow still evolves until a new equilibrium profile characterized by  $\ln(z_0 + z_d) \approx 3$  is found at  $x \approx 120$  m. This new condition holds until to  $x \approx 450$  m, where the flow experiences an abrupt rough to smooth roughness transition.

The values of  $\ln(z_0 + z_d)$  estimated in Figure 12 as well as the downstream positions at which they vary are in reasonable agreement with the morphometric values data obtained in Test2S, thus confirming the strength of the morphometric approach proposed in this paper. Note that only spanwise averaged profiles of mean velocities were available; therefore, the comparison is done only against the 1D tests. Specifically, Test2S was chosen as it allowed a more fine-scale comparison with the CFD results.

### Implications: determination of the in-canopy velocity scale

Previous studies have shown the potential of morphometric methods for the modelling of the low-level mean urban flow through the concept of in-canopy velocity,  $U_c$ , a velocity scale representing a sort of spatially averaged advection velocity within the building array (Bentham & Britter, 2003). In this respect, the ability of computing scale-adaptive morphometric parameters using the image-based morphometric method presented here is a step forward because it allows the estimation of a local value of  $U_c$ , namely, significant local changes in urban ventilation induced by geometrical heterogeneities within a certain neighbourhood or between adjacent neighbourhoods (Panagiotou et al., 2013).

To illustrate this concept, the in-canopy velocity is evaluated from the CFD simulations (hereafter  $U_{c,CFD}$ ) and compared with morphometry-based formulations of  $U_c$  available in the literature. Only one DEM partition is discussed here (Test2S), as the purpose is merely illustrative.

Several expressions for the in-canopy velocity exist in the literature obtained using data from laboratory experiments and numerical simulations of flow over cube arrays and in few cases over urban areas with relatively low height variability. To the authors' knowledge, this

is the first attempt where the concept of in-canopy velocity is tested for a highly inhomogeneous urban geometry, which is typical of many US city downtowns as well as the majority of megacities around the world.

According to Bentham and Britter (2003):

$$\frac{U_C}{u_*} = \sqrt{\frac{2}{\lambda_f}} \quad \text{for } \lambda_f > 0.2 \quad (4a)$$

$$\frac{U_C}{u_*} = \sqrt{\frac{2\bar{H}}{z_0}} \quad \text{for } \lambda_f < 0.2 \quad (4b)$$

A modification to equation (4b) was proposed by Solazzo et al. (2010) to account for the area occupied by the building:

$$\frac{U_C}{u_*} = (1 - \lambda_p) \sqrt{\frac{2}{\lambda_f}} \quad (4c)$$

The three models were evaluated for Test2S and compared against  $U_{c,CFD}$ , which represents the CFD mean velocity averaged horizontally on each DEM portion shown in Test2S ( $\langle U(z) \rangle$ ) and vertically from ground up to  $z = \bar{H}$ , where  $\bar{H}$  is the average building height associated with each DEM portion. The friction velocity  $u_*$  was derived from the equation (3) LOG profile by evaluating  $\langle U(z) \rangle$  at a reference height  $z = 2.5\bar{H}$ .

The results are summarized in Table 2 and Figure 13 (a), which show that the best agreement is found for equation (4a) regardless of the value  $\lambda_f$ , while the worst agreement is for equation (4b).

Using this simple formula for  $U_C$ , it is possible to evaluate the deceleration of flow through the canopy (Figure 13(b)), thus giving an indication of the time of residence of a given scalar (heat, pollutants) in a certain neighbourhood or intra-neighbourhood area. Besides, once  $U_C$  is known, the computation of the exchange velocity is straightforward (Bentham & Britter, 2003; Solazzo et al., 2010). Thus, the method guides one to identify areas of potential thermal discomfort and poor air quality and to evaluate the efficiency of urban planning strategies or urban renewal projects (e.g. ventilation corridors, new building location).

**Table 2.** Comparison between  $U_{c,CFD}$  and  $U_c$  based on equations (4a–c) and their combinations. The mean relative error  $|U_{c,CFD} - U_c| / U_{c,CFD}$  and its standard deviation are provided for Test2S.

	Equation (4a) (any $\lambda_f$ )	Equation (4b) (any $\lambda_f$ )	Equation (4c) (any $\lambda_f$ )	Equations (4a) (for $\lambda_f > 0.2$ ) and (4b) (for $\lambda_f < 0.2$ )	Equations (4c) (for $\lambda_f > 0.2$ ) and (4b) (for $\lambda_f < 0.2$ )
Mean relative error (%)	29	121	32	105	111
Standard deviation	23	109	21	117	113

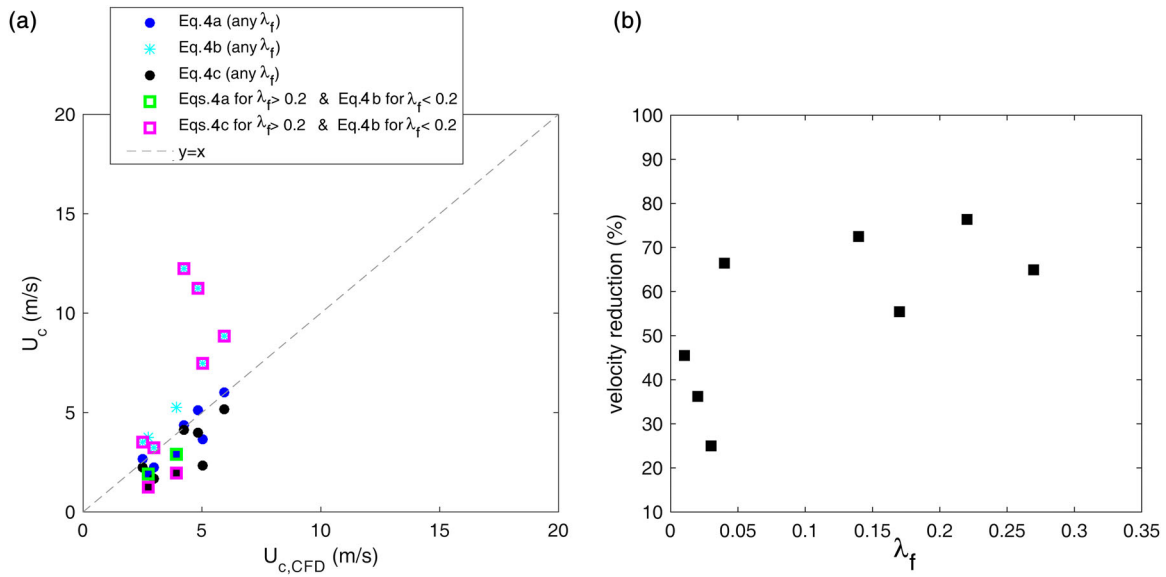


**Figure 13.** (a) In-canopy velocity  $U_C$  based on equations (4a–c) and their combinations versus computational fluid dynamics (CFD) estimation. (b) Velocity reduction for Oklahoma City as a function of intra-domain lambda variations (see the methodology section). Velocity reduction was evaluated as  $|U_{o,C} - U_C| / U_{o,C}$ , where  $U_{o,C}$  denotes the CFD upstream profile  $U_o$  averaged from the ground to  $z = \bar{H}$ .

**Implications: sensitivity to DEM grid spacing and aerodynamic roughness length formulations**

Normalized concentration  $K$  obtained from the ADMS-Urban are compared here with WT measurements for the four runs described above in the method section.

Specifically, the image-based analysis was carried out on regular grids consisting of  $2 \times 2$  (TestR1),  $3 \times 3$  (TestR2)

and  $4 \times 4$  (TestR3) regions respectively, as well as on regularly spaced partitions consisting of  $3 \times 2$  (TestR4) and  $4 \times 3$  (TestR5) sub-regions (Figure 14) to assess the effect of the image-based grid spacing on ADMS performances. Note that TestR4 and TestR5 are similar to Test3 and Test3b in terms of number of sub-regions, but the image-based grid spacing is not regular in the latter two.

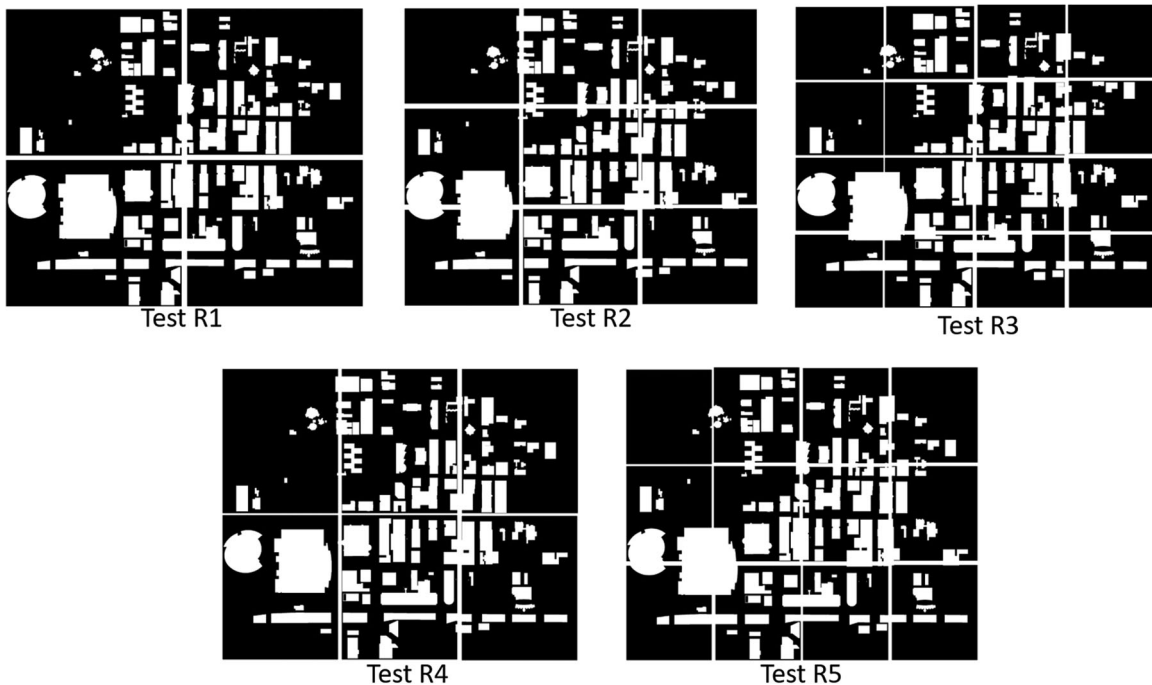


**Figure 14.** Grid adopted for the Oklahoma City geometry in TestsR1–R5.

ADMS/WT comparison at different regular grid spacing (TestsTR1–TR5) indicates that at lower elevation ( $z \leq 6$  m), the coarsest resolution (TR1 followed by TR4) gives the best results and the peak value of concentration is reasonably well captured. The agreement decreases as the grid resolution increases. At highest elevation ( $z = 12$  m), however, the agreement is generally worse with no significant differences among the tests (Figure 15). The same trend is also found when comparing the irregular DEM partitions (Test3 versus Test3b) based on the horizontal variation of  $\sigma_H/\bar{H}$  and  $H_m/H_{\max}$ , with the finer grid (dictated by  $\sigma_H/\bar{H}$ ) having worse agreement (Figure 16). For reference, Test1 is also plotted in Figure 16, which has the poorest agreement among all the tests, as expected.

Taking TR1 as benchmark case, different roughness formulations were then evaluated (Figure 17): at lower elevation ( $z \leq 6$  m), [KA1] and [KA2] lead to a significant underestimation of the peak concentration, which is reasonably well captured by [MA]. Note that [MA] and [KR] provide almost identical profiles. Again, the situation is different at  $z = 12$  m, where the agreement is generally worse.

Finally, Figure 18 aims at comparing the different approaches discussed in this paper, again using TR1 as

the benchmark. Specifically, we consider the results from our methodology using a DEM grid spacing based on (1) information of building height variability (Test3); (2) information on the street network (Test3S); and (3) a regular coarse grid, as well as the results from application of a wavelet method (lev7). Surprisingly, Test3S (which has the finest DEM grid spacing) performs comparably well with TestR1 (coarse regular grid), and has better agreement with WT data especially closer to the source and at a higher elevation. This is also confirmed by the statistics given in Table 3, which shows the statistical parameters mean, standard deviation, maximum, normalized mean square error (NMSE), FAC2, fractional bias (FB) and  $R$ . Test3S captures better the concentration peak as well as the horizontal spread (standard deviation) in concentration; further, it was the only test that also simultaneously mostly fulfils the recommended criteria, *i.e.*  $NMSE \leq 1.5$ ,  $FAC2 \geq 0.5$  and  $-0.3 \leq FB \leq 0.3$  (Di Sabatino et al., 2011).

## Discussion

The grid sensitivity analysis carried out above suggests that better model performances are achieved at coarser resolution either on regular (TestsR1–R5) and irregular

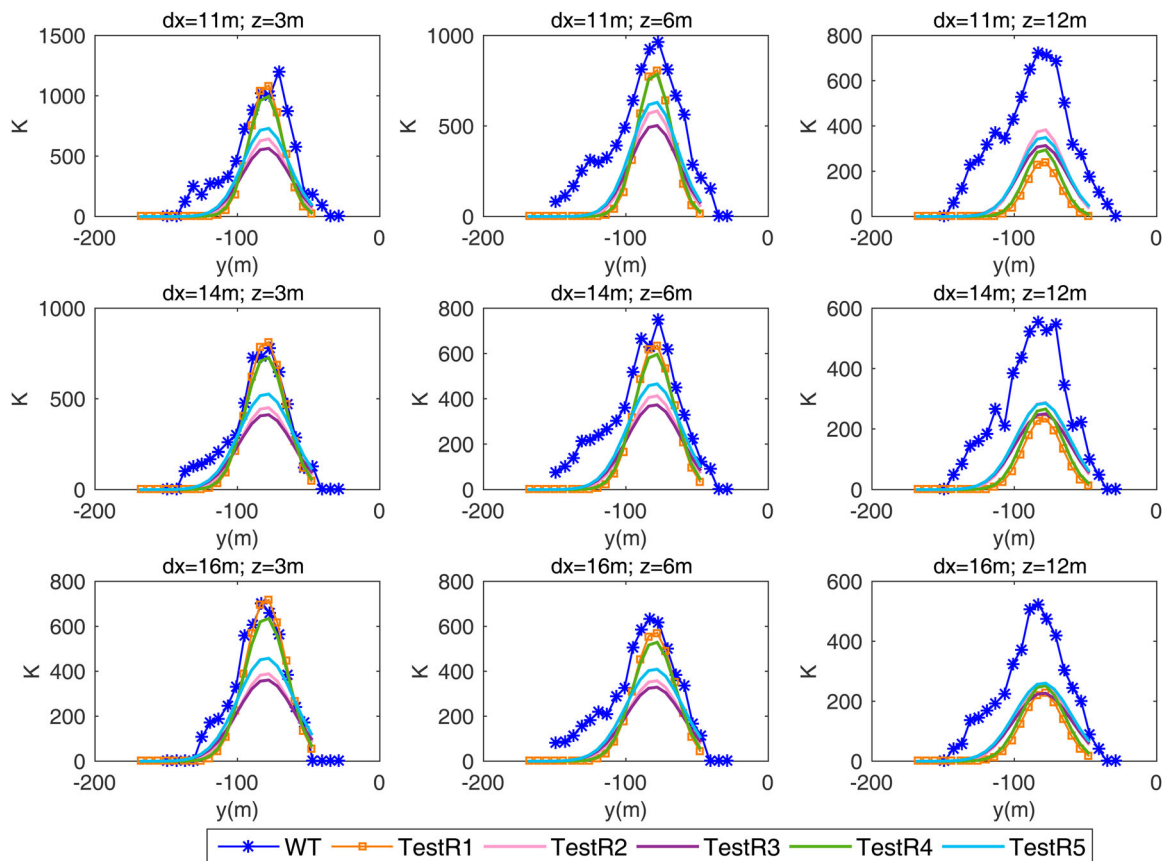


**Figure 15.** Horizontal profiles of normalized concentration  $K$  from wind tunnel (WT) and ADMS-Urban runs for TestsR1–R5 at several distances  $dx$  from the source and heights  $z$ .



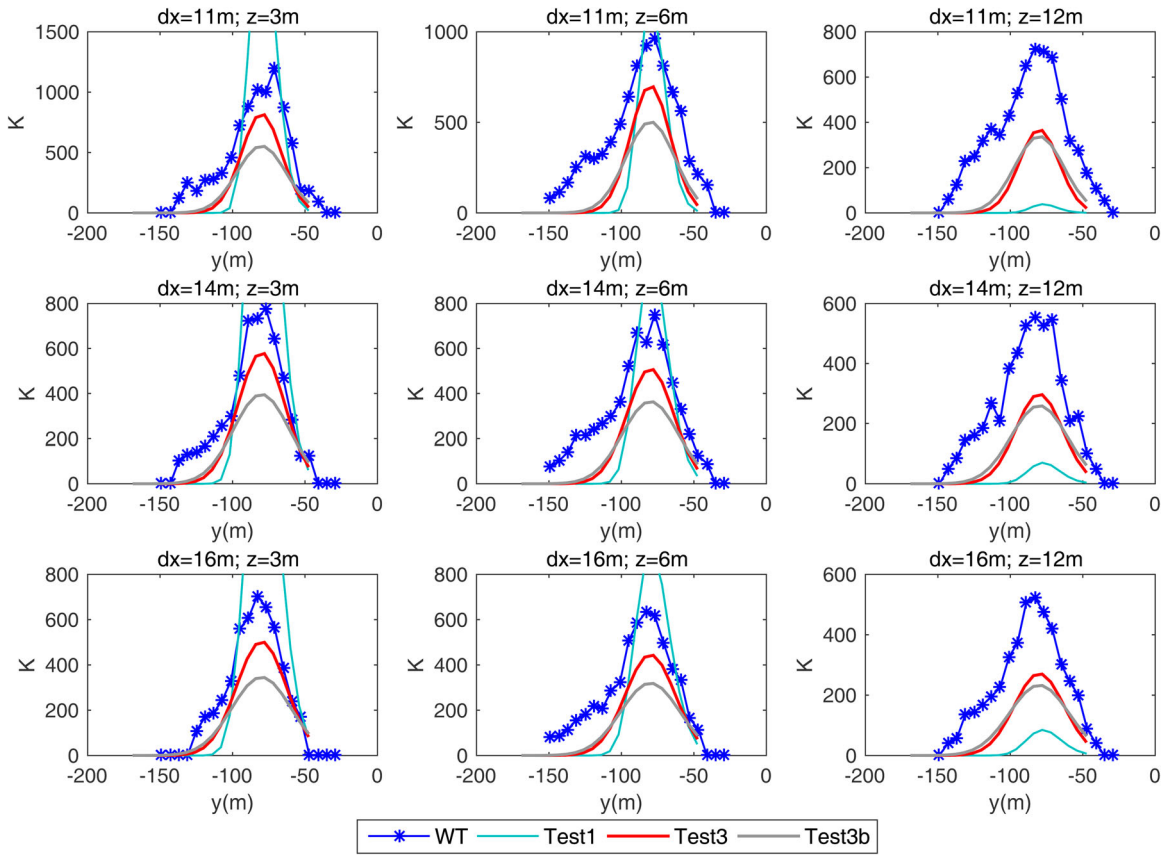


Figure 16. Same as for Figure 15 but for Test1, Test3 and Test3b.

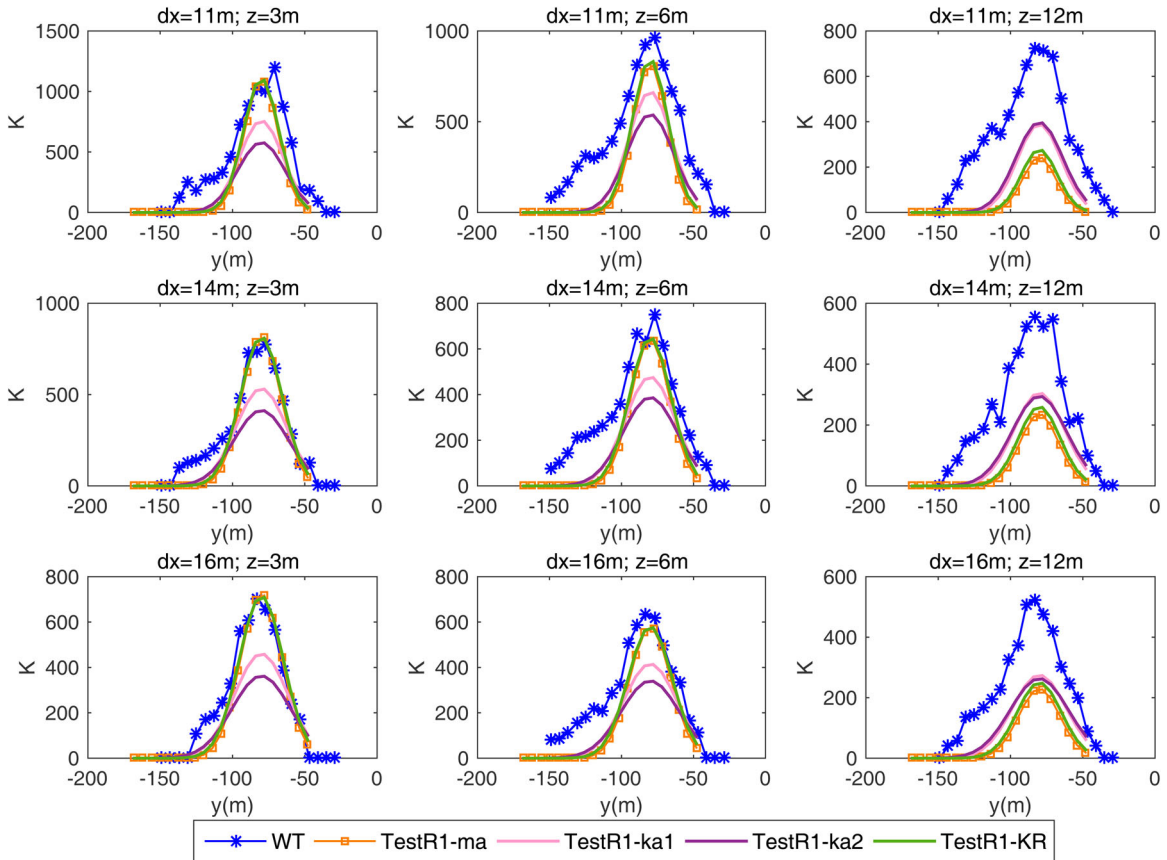
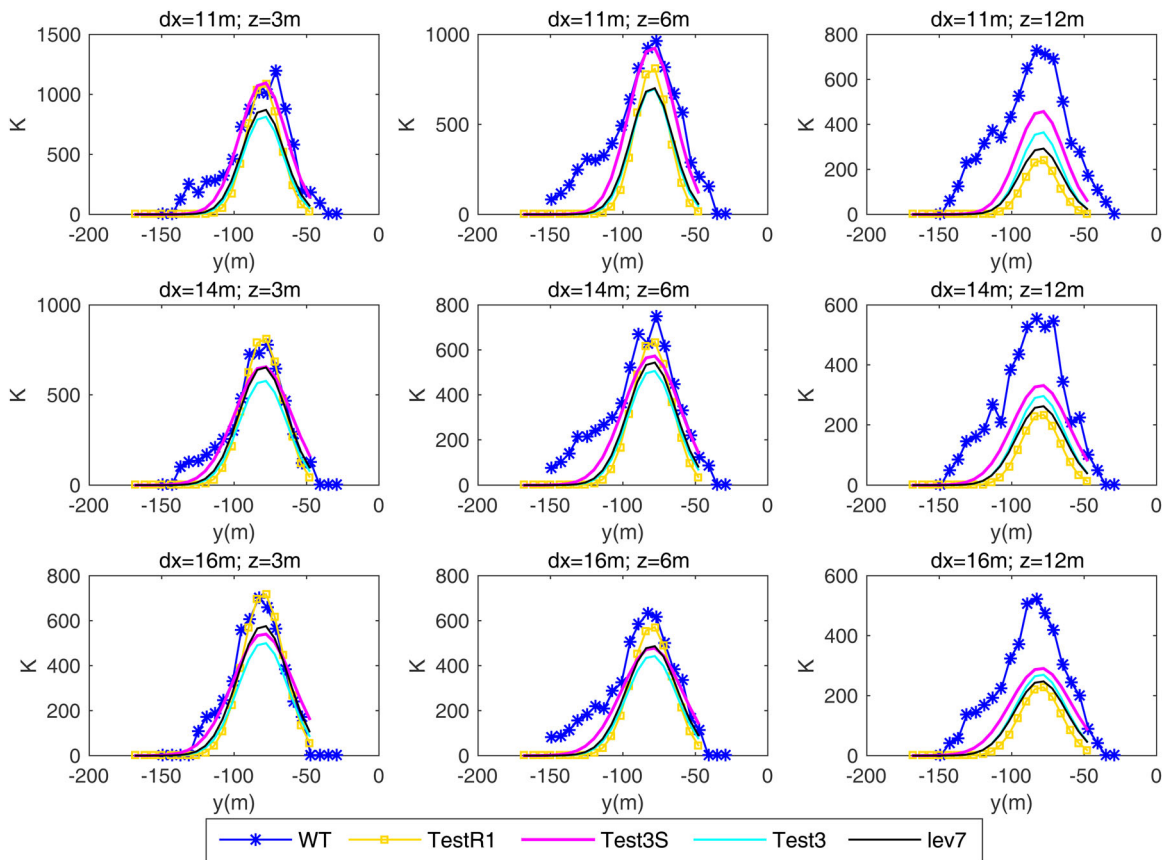


Figure 17. Same as for Figure 15 but for TestR1 and different  $z_0$  formulations.



**Figure 18.** Same as for Figure 15 but for Test3, Test3S and lev7.

(Test3 versus Test3b) grids. Nevertheless, when the street grid is adopted, even a much finer scale grid such the one of Test3S outperforms all the others, regardless of the grid resolution (Test3S performs better than either the coarser grids such as TestR1 or finer grids such as lev7) or the type of grid (regular versus irregular partitions). This result implies that for numerical dispersion model applications that consider intra-city scales (neighbourhood scale) and/or when the goal is to evaluate the model performances with point measurements of concentration taken within or along street canyons (which is what usually exists in real situation), positioning of the grid along the street is the right choice. When extending this approach to urban neighbourhoods larger than OKC (or with a much denser street network), which streets (and therefore grid spacing) to choose can be then guided by the profile of  $H_m/H_{max}$ . This is because the roughness elements (sub-regions of size  $\Delta x$ ,  $\Delta y$ ) would be positioned closer to the actual positions of those building that contribute more to the final  $z_{01}$ ,  $z_{02}$  etc. over the domain. This hypothesis, however, will need further validation. It is also worth noting that the above interpretation and conclusions were drawn focusing on neighbourhood-scale applications. When using a model tailored for the entire city scale, the criterion

based on  $\sigma_H/\bar{H}$  may be the optimum choice instead. This is because for models at this coarser resolution, the correct positioning of the roughness elements is less crucial than building height variability. It is therefore evident that to guide the choice for the calculation of morphometric parameters, it is not the resolution per se that is important but rather the physics being represented by the specific numerical model being used. Physical boundaries, e.g. those surfaces characterized by homogeneous morphometric characteristics and used in mesoscale models, are those that determine the grid size. Geometric boundaries, e.g. streets networks, are those to be used in finer resolution models or in those such as ADMS type models where the street canyon scale is explicitly accounted for.

## Conclusions

This paper presents a novel method for the estimation of adaptive-scale morphometric parameters starting from detailed building data and employing an image-based technique. Previous studies (Di Sabatino et al., 2010) have shown that by computing five morphometric parameters, namely  $\lambda_p$ ,  $\bar{H}$ ,  $H_{max}$ ,  $\lambda_f$  and  $\sigma_H$ , as a function of the elevation  $z$  the bulk essence of the urban form is

**Table 3.** Characteristics of each test and statistical metrics comparing concentrations obtained from ADMS-Urban with wind tunnel (WT) data at the measurement positions.

Test	Grid	Digital elevation model (DEM) partition criteria	Sensitivity analysis on:			WT (average/SD/maximum)	ADMS (average/SD/maximum)	NMSE	FB	R	FAC2
			Grid resolution	$z_0$ formulae	Partition criteria						
R1	Regular 2 × 2	Regular grid	*	*	*	341/251/1199	179/246/1085	0.69	0.63	0.87	0.30
R1 ka1				*			181/185/752	0.58	0.61	0.94	0.50
R1 ka2				*			162/1/575	0.85	0.71	0.94	0.46
R1 KR				*			195/252/1093	0.54	0.55	0.88	0.38
R2	Regular 3 × 3	Regular grid	*				160/161/643	0.84	0.72	0.94	0.41
R3	Regular 4 × 4	Regular grid	*				153/143/564	0.99	0.76	0.93	0.35
R4	Regular 3 × 2	Regular grid	*				181/230/996	0.62	0.62	0.90	0.36
R5	Regular 4 × 3	Regular grid	*				185/180/730	0.57	0.59	0.93	0.50
1	//	//	*				245/475/2477	1.45	0.33	0.74	0.23
2	Irregular 3 × 1	$H_m(x)/H_{max}$					184/239/1043	0.61	0.60	0.89	0.35
2S	Irregular 8 × 1	$H_m(x)/H_{max} = 0$					182/212/896	0.57	0.61	0.92	0.41
3	Irregular 3 × 3	$H_m(x,y)/H_{max}$	*		*		177/195/813	0.62	0.64	0.93	0.44
3b	Irregular 5 × 3	$(H_m(x,y)/H_{max}, \sigma_H/\bar{H})$	*				154/141/551	0.98	0.76	0.94	0.35
3S	Irregular 8 × 4	$H_m(x,y)/H_{max} = 0$			*		244/247/1095	0.22	0.33	0.93	0.63
lev	Regular 9 × 8	Wavelet			*		189/211/871	0.54	0.58	0.90	0.42

Notes: Sensitivity analyses conducted on various tests and discussed in the main text are indicated by an asterisk (\*), with the best performance being that for Test3S.

FAC2 = fraction of predictions within a factor of two of observations; FB = fractional bias; NMSE = normalized mean square error; R = correlation coefficient; SD = standard deviation; // means that no DEM partition was applied.

captured. The authors have proved that the method can be generalized to calculate the 2D distribution of the morphometric parameters, while accounting for the vertical building height distribution. The change from 1D to 2D introduces an intrinsic difficulty associated with the right choice of the grid used for the calculation of the morphometric parameters. It was shown that such a grid can be used by adopting some simple rules associated with the ratios  $\sigma_H/\bar{H}$  and  $H_m/H_{\max}$ . Specifically, the method has been built for applications to inhomogeneous urban geometries for which it is thus not obvious to extrapolate appropriate urban canopy parameterizations.

To this aim, the method was applied to the real test case of downtown OKC. First, the fluid dynamics relevance of the calculated aerodynamic parameters was assessed by comparison with results obtained from high-resolution CFD simulations. Second, the estimated morphometric parameters were employed to obtain information on urban ventilation characteristics at the neighbourhood scale. The application showed that the horizontal transport of scalars and pollutants within a city and among adjacent neighbourhood mainly depends on the frontal area density of a given neighbourhood. Therefore, the computation of such parameters at intra-urban scales may guide urban planners to identify ventilation corridors versus building arrangements, leading to more stagnant air conditions. Third, improvements in the performance of an operational dispersion model using spatially varying aerodynamic roughness length estimated by morphometric parameters were evaluated against WT data. The selected application showed that it is crucial to account for finer scale morphometric variations in such dispersion models to obtain accurate concentration predictions. This specific application also showed the performance of several formulations of  $z_0$  existing in the literature. Three formulations were tested, namely Macdonald et al. (1998), Kastner-Klein and Rotach (2004) and Kanda et al. (2013), showing that both [MA] and [KR] give the best results.

To guide potential users of this method and to further highlight the consequences of this study, the following are emphasized:

- the use of morphometric parameters based on scale-adaptive methods provide better agreement with measured data than those in which scales for their calculations are arbitrarily chosen
- the scale chosen for the calculation of morphometric parameters is model dependent
- morphometric parameters should be calculated by positioning the computational grid based on *physical*

*boundaries*, while for finer resolution (namely, smaller scale) numerical models, morphometric parameters should be calculated using the street grid as an external boundary, and the maximum building height criterion performs well

While the present study shows the great potential of this new method, it also calls for a more robust validation and further generalization by looking at larger urban domains, cities having morphometric characteristics different from OKC (e.g. European cities), additional experimental data sets and CFD simulations.

### Disclosure statement

No potential conflict of interest was reported by the authors.

### Funding

The third author (SDS) kindly acknowledges the iSCAPE (Improving Smart Control of Air Pollution in Europe) project, which is funded by the European Community's H2020 Programme (H2020-SC5-04-2015) under the Grant Agreement No. 689954.

### ORCID

Laura S. Leo  <http://orcid.org/0000-0003-4103-6862>

Riccardo Buccolieri  <http://orcid.org/0000-0002-0102-7235>

Silvana Di Sabatino  <http://orcid.org/0000-0003-2716-9247>

### References

- Aliabadi, A. A., Krayenhoff, E. S., Nazarian, N., Chew, L. W., Armstrong, P. R., Afshari, A., & Norford, L. K. (2017). Effects of roof-edge roughness on air temperature and pollutant concentration in urban canyons. *Boundary-Layer Meteorology*, 164, 249–279.
- Barlow, J. F. (2014). Progress in observing and modelling the urban boundary layer. *Urban Climate*, 10, 216–240.
- Barnes, M. J., Brade, T. K., MacKenzie, A. R., Whyatt, J. D., Carruthers, D. J., Stocker, J., ... Hewitt, C. N. (2014). Spatially-varying surface roughness and ground-level air quality in an operational dispersion model. *Environmental Pollution*, 185, 44–51.
- Bentham, T., & Britter, R. (2003). Spatially averaged flow within obstacle arrays. *Atmospheric Environment*, 37, 2037–2043.
- Blocken, B., Tominaga, Y., & Stathopoulos, T. (2013). CFD simulation of micro-scale pollutant dispersion in the built environment. *Building and Environment*, 64, 225–230.
- Britter, R. E., & Hanna, S. R. (2003). Flow and dispersion in urban areas. *Annual Review of Fluid Mechanics*, 35, 469–496.
- Buccolieri, R., Salizzoni, P., Soulhac, L., Garbero, V., & Di Sabatino, S. (2015). The breathability of compact cities. *Urban Climate*, 13, 73–93.
- Buccolieri, R., Sandberg, M., & Di Sabatino, S. (2010). City breathability and its link to pollutant concentration



- distribution within urban-like geometries. *Atmospheric Environment*, 44, 1894–1903.
- Buccolieri, R., Wigö, H., Sandberg, M., & Di Sabatino, S. (2017). Direct measurements of the drag force over aligned arrays of cubes exposed to boundary-layer flows. *Environmental Fluid Mechanics*, 17, 373–394.
- Carruthers, D., Di Sabatino, S., & Hunt, J. R. C. (2012). Urban air quality urban air quality: Meteorological processes urban air quality meteorological processes. In R. A. Meyers (Ed.), *Encyclopedia of sustainability science and technology* (pp. 11262–11291). Springer-Verlag New York: Springer Science+ Business Media.
- CERC. (2017). ADMS-Urban user guide. Retrieved from [http://cerc.co.uk/environmental-software/assets/data/doc\\_userguides/CERC\\_ADMS-Urban4.1.1\\_User\\_Guide.pdf](http://cerc.co.uk/environmental-software/assets/data/doc_userguides/CERC_ADMS-Urban4.1.1_User_Guide.pdf)
- Ching, J., See, L., Mills, G., Alexander, P., Bechtel, B., Feddema, J., ... Wang, X. (2014). WUDAPT: Facilitating advanced urban canopy modeling for weather, climate and air quality applications. *Urban Climate News*, 45, 6–17.
- Di Sabatino, S., Buccolieri, R., & Kumar, P. (2018). Spatial distribution of air pollution in cities. In F. Capello, & A. Gaddi (Eds.), *Clinical handbook of air pollution-related diseases* (pp. 75–95). Cham: Springer.
- Di Sabatino, S., Buccolieri, R., Olesen, H. R., Ketzler, M., Berkowicz, R., Franke, J., ... Starchenko, A. (2011). COST 732 in practice: The MUST model evaluation exercise. *International Journal of Environment and Pollution*, 44, 403–418.
- Di Sabatino, S., Leo, L. S., Cataldo, R., Ratti, C., & Britter, R. (2010). Construction of digital elevation models for a southern European city and a comparative morphological analysis with respect to northern European and north American cities. *Journal of Applied Meteorology and Climatology*, 49, 1377–1396.
- Di Sabatino, S., Solazzo, E., Paradisi, P., & Britter, R. (2008). A simple model for spatially-averaged wind profiles within and above an urban canopy. *Boundary-Layer Meteorology*, 127, 131–151.
- Fernando, H. J. S. (2000). Fluid dynamics of urban atmospheres in complex terrain. *Annual Review of Fluid Mechanics*, 42, 365–389.
- Grimmond, C. S. B., & Oke, T. R. (1999). Aerodynamic properties of urban areas derived from analysis of surface form. *Journal of Applied Meteorology*, 38, 1262–1292.
- Jackson, P. S. (1981). On the displacement height in the logarithmic velocity profile. *Journal of Fluid Mechanics*, 111, 15–25.
- Jackson, P. S., & Hunt, J. C. R. (1975). Turbulent wind flow over a low hill. *Quarterly Journal of the Royal Meteorological Society*, 101, 929–955.
- Kaimal, J. C., & Finnigan, J. J. (1994). *Atmospheric boundary layer flows: Their structure and measurement*. Oxford: Oxford University Press, 289 pp.
- Kanda, M., Inagaki, A., Miyamoto, T., Gryschka, M., & Raasch, S. (2013). A new aerodynamic parametrization for real urban surfaces. *Boundary-Layer Meteorology*, 148, 357–377.
- Kastner-Klein, P., & Rotach, M. W. (2004). Mean flow and turbulence characteristics in an urban roughness sublayer. *Boundary-Layer Meteorology*, 111, 55–84.
- Kent, C. W., Grimmond, S., Barlow, J., Gatey, D., Kotthaus, S., Lindberg, F., & Halios, C. H. (2017). Evaluation of urban local-scale aerodynamic parameters: Implications for the vertical profile of wind speed and for source areas. *Boundary-Layer Meteorology*, 164, 183–213.
- Krayenhoff, E. S., Santiago, J.-L., Martilli, A., Christen, A., & Oke, T. R. (2015). Parametrization of drag and turbulence for urban neighbourhoods with trees. *Boundary-Layer Meteorology*, 156, 157–189.
- Kubilay, A., Neophytou, M. K.-A., Matsentides, S., Loizou, M., & Carmeliet, J. (2017). The pollutant removal capacity of urban street canyons as quantified by the pollutant exchange velocity. *Urban Climate*, 21, 136–153.
- Lauder, B. E., & Spalding, D. (1974). The numerical computation of turbulent flows. *Computer Methods in Applied Mechanics and Engineering*, 3, 269–289.
- Leitl, B., Pascheke, F., Schatzmann, M., & Kastner-Klein, P. (2003). *Wind tunnel experiments within the scope of the Oklahoma City tracer experiments*. Proc. int. workshop on physical modelling of flow and dispersion phenomena PHYSMOD2003, Prato, Italy, September 3–5.
- Liu, C. H., Ng, C. T., & Wong, C. C. C. (2015). A theory of ventilation estimate over hypothetical urban areas. *Journal of Hazardous Materials*, 296, 9–16.
- Macdonald, R. W., Griffiths, R. F., & Hall, D. J. (1998). An improved method for the estimation of surface roughness of obstacle arrays. *Atmospheric Environment*, 32, 1857–1864.
- Martilli, A., Santiago, J. L., & Salamanca, F. (2015). On the representation of urban heterogeneities in mesoscale models. *Environmental Fluid Mechanics*, 15, 305–328.
- Millward-Hopkins, T., Tomlin, A. S., Ma, L., Ingham, D. B., & Pourkashanian, M. (2013). Aerodynamic parameters of a UK city derived from morphological data. *Boundary-Layer Meteorology*, 146, 447–468.
- Ming, T., Peng, C., Gong, T., & Li, Z. (2017). *Pollutant dispersion in built environment*. Singapore: Springer.
- Mouzourides, P., Kyprianou, A., Brown, M. J., Carissimo, B., Choudhary, R., & Neophytou, M. K.-A. (2014). Searching for the distinctive signature of a city in atmospheric modelling: Could the multi-resolution analysis (MRA) provide the DNA of a city? *Urban Climate*, 10, 447–475.
- Mouzourides, P., Kyprianou, A., & Neophytou, M. A. (2013). A scale-adaptive approach for spatially-varying urban morphology characterization in boundary layer parametrization using multi-resolution analysis. *Boundary-Layer Meteorology*, 149, 455–481.
- Nishizawa, S., Sawachi, T., & Maruta, E. (2008). *Evaluation of effect of the wind pressure fluctuation for cross ventilation in the residential district*. Proc. Air infiltration and ventilation centre conference, Kyoto, Japan.
- Oke, T. R. (1987). *Boundary layer climates* (2nd ed.). London: Methuen.
- Panagiotou, I., Neophytou, M. K.-A., Hamlyn, D., & Britter, R. E. (2013). City breathability as quantified by the exchange velocity and its spatial variation in real inhomogeneous urban geometries: An example from central London urban area. *Science of The Total Environment*, 442, 466–477.
- Ratti, C., Di Sabatino, S., & Britter, R. (2006). Analysis of urban texture with image processing techniques: Winds and dispersion. *Theoretical and Applied Climatology*, 84, 77–90.

- Roth, M. (2000). Review of atmospheric turbulence over cities. *Quarterly Journal of the Royal Meteorological Society*, 126, 941–990.
- Salizzoni, P., Soulhac, L., & Mejean, P. (2009). Street canyon ventilation and atmospheric turbulence. *Atmospheric Environment*, 43, 5056–5067.
- Schatzmann, S., Olesen, H., & Franke, J. (2010). COST 732 model evaluation case studies: approach and results. Retrieved from [www.cost.eu/COST\\_Actions/essem/732](http://www.cost.eu/COST_Actions/essem/732)
- Solazzo, E., Di Sabatino, S., Aquilina, N., Dudek, A., & Britter, R. (2010). Coupling mesoscale modelling with a simple urban model: The Lisbon case study. *Boundary-Layer Meteorology*, 137, 441–457.
- Soulhac, L., Salizzoni, P., Mejean, P., & Perkins, R. J. (2013). Parametric laws to model urban pollutant dispersion with a street network approach. *Atmospheric Environment*, 67, 229–241.
- Tennekes, H. (1973). The logarithmic wind profile. *Journal of the Atmospheric Sciences*, 30, 234–238.
- Tominaga, Y., & Stathopoulos, T. (2013). CFD simulation of near-field pollutant dispersion in the urban environment: A review of current modeling techniques. *Atmospheric Environment*, 79, 716–730.
- Wang, Q., Sandberg, M., Lin, Y., Yin, S., & Hang, J. (2017). Impacts of urban layouts and open space on urban ventilation evaluated by concentration decay method. *Atmosphere*, 8, 169.
- Wiernga, J. (1993). Representative roughness parameters for homogeneous terrain. *Boundary-Layer Meteorology*, 63, 323–363.
- Xie, Z.-T., Coceal, O., & Castro, I. P. (2008). Large-eddy simulation of flows over random urban-like obstacles. *Boundary-Layer Meteorology*, 129, 1–23.